

Multi-Epoch Observations of the Nearby Spiral Galaxy NGC 3938 with the *Chandra* X-ray Observatory

SIDDHI RAUT,¹ ERIC M. SCHLEGEL,² THOMAS G. PANNUTI,³ BRANNON W. JONES,³ AND JACOBO MATA LLANA³

¹Ronald Reagan High School, 19000 Ronald Reagan, San Antonio, TX 78258, USA^a

²Department of Physics and Astronomy, University of Texas at San Antonio, One UTSA Circle, San Antonio, TX 78249 USA

³Department of Engineering Science, 123 Lappin Hall, Morehead State University, 150 University Drive, Morehead, KY 40351, USA

ABSTRACT

We present an analysis of two epochs of ACIS observations of the SA(s)c spiral galaxy NGC 3938 with the *Chandra* X-ray Observatory. The total exposure time of the observations was 95 ksecs with a limiting unabsorbed luminosity of $\approx 10^{38}$ ergs/sec assuming a distance of 22 Mpc. A total of 47 discrete merged sources from both epochs were detected at the $\approx 3\sigma$ level or greater with the D25 radius. We demonstrate that at the time of the *Chandra* observations, the nucleus was *not* detected. We connect the detected sources to counterparts in other wavebands to the degree possible. Based on the two epochs, we identify three variable sources and an additional two that may have varied between the two observations. We do not formally detect any of the five historical supernovae that have occurred in NGC 3938. The luminosity function of NGC 3938 is compared to a recent compilation of 38 galaxies and we identify a potentially significant problem with the ‘known’ distance to NGC 3938. Star formation rate and metallicity values are also computed; the star formation rate is highly dependent upon the adopted distance. The metallicity appears to lie in the range of 8.2-9.2, consistent with values from other work. We include in an appendix a short discussion of the sources that lie in *Chandra*’s field-of-view but lie outside of NGC 3938.

Keywords: X-ray sources (1822) — Spiral galaxies (1560) – X-ray astronomy (1810)

1. INTRODUCTION

The *Chandra* X-ray Observatory’s sharp point spread function has yielded advances of our understanding of the properties of discrete X-ray sources (e.g., X-ray binaries (XRBs) (e.g., Lehmer et al. (2021); Binder et al. (2017); Mineo et al. (2012)); supernova remnants (SNRs) (e.g., Sasaki (2020)) in nearby galaxies. The as-yet unsurpassed angular resolution of *Chandra* of $\sim 1''$ (van Speybroeck et al. (1997), Gaetz et al. (2000)) has led to an increase in the number of discrete X-ray sources for which variability analyses and positional accuracy aid in the identification of possible counterparts at other wavelengths (particularly the infrared and radio wavelengths).

The X-ray sources within a galaxy are often connected to stellar evolution, either as SNRs or XRBs. By observing the XRBs and SNRs in other galaxies, greater insight can be provided about our own, the Milky Way. Interstellar dust within the Milky Way prevents linking many sources across the electromagnetic spectrum whereas nearby, face-on spirals permit a uniform survey of X-ray-emitting sources.

The study of galaxies in the X-ray band typically breaks in two directions: the study of X-ray-emitting objects in the galaxy or the study of the nucleus. Much of that break is driven by the distances to individual galaxies. The *Einstein* generation of detectors could resolve a few very nearby galaxies into *any* individual sources; all others were essentially

siddhi.raut.missionartemis@gmail.com

eric.schlegel@utsa.edu

t.pannuti@moreheadstate.edu

^a Currently an undergraduate at the University of Chicago

an unresolved blur (Fabbiano, Kim, & Trinchieri 1992). *ROSAT*, with its improved spatial resolution, permitted a larger volume to be investigated before sources became too confused, allowing the first identifications of individual sources, e.g., ultra-luminous X-ray sources (ULX; Zampieri (2006)). *Chandra* allows the study of individual sources in galaxies to ≈ 5 Mpc. That resolution also permits pushing the outer boundary outward to ≈ 20 -25 Mpc at which point most sources are confused or blurred together. Within that volume lies the face-on unbarred SA(s)c galaxy NGC 3938.

NGC 3938 has a low-luminosity nucleus hence the LINER classification (LINER = Low Ionization Nuclear Emission Region; Pellegrini et al. (2000), Ho et al. (1997)). It is one of the brightest in the Ursa Major South galaxy group at an inclination angle of $i \sim 14^\circ$ (JimenezVicente et al. 1999). A previous, 50 ksec study of NGC 3938 using *Chandra* detected ~ 45 sources within the D25 radius¹ (Buhidar & Schlegel 2017). Regions of star formation in NGC 3938 have also been observed through the near-ultraviolet (NUV) from GALEX², H α from JKT³ and KPNO⁴, 8 and 24 μm from *Spitzer*, and CO from BIMA⁵ which resulted in an obtained power-law relationship between the emission region volume and luminosity (Caldú-Primo et al. 2009). Five supernovae have erupted in NGC 3938: SN 2017ein is a progenitor candidate for the Type Ic supernova (Van Dyk et al. 2017) along with four other supernovae: SN 1961U (SN IIL), SN 1964L (SN Ib), SN 2005ay (SN IIP), and SN 2022xlp (SN Iax).

NGC 3938 visibly lacks nearby neighbors, suggesting a relatively isolated galaxy. However, it is useful to note that NGC 3938 is part of the Ursa Major South galaxy group, so it is isolated to a certain extent. NGC 3938 lies at a “preferred” distance, according to the NASA Extragalactic Database⁶(hereafter, NED), of 15.3 Mpc. However, that distance is based essentially on a mean value of measured distances that differ substantially. Recent measures fall in the 17 (Poznanski et al. 2009) to 22 (Rodriguez et al. 2014) Mpc range. We initially adopted 22 Mpc as the distance to NGC 3938. That places the galaxy at essentially the outer edge of a volume in which *Chandra* will return a starting census of the X-ray-emitting objects: an object emitting of order 10^{38} ergs s^{-1} will produce a few counts in a 50-ksec exposure at that distance. However, we return to a short discussion of the distance in §8 and its possible ‘incorrectness’ when describing the distribution of source counts with luminosity.

We describe and characterize two observations of the NGC 3938 obtained by the *Chandra* X-ray Observatory. The data from the two epochs was also examined for counterparts at other wavelengths.

The paper is organized in this matter: Section 2 describes the observations and data reductions. Section 3 delves into the specific sources and their detection. X-ray properties derived from color-color hardness are then discussed in Section 4, and Sections 5 and 6 talk about time-variable emission and multi-wavelength source comparison respectively. Section 7 will detail the star formation rate and metallicity of NGC 3938, and Section 8 will summarize our results and conclusions.

¹ The diameter at which the surface brightness of the galaxy in an optical band has fallen to mag 25 / arcsec².

² Galaxy Evolution Explorer, Bianchi (2014)

³ Jacobus Kapteyn Telescope, La Palma

⁴ Kitt Peak National Observatory

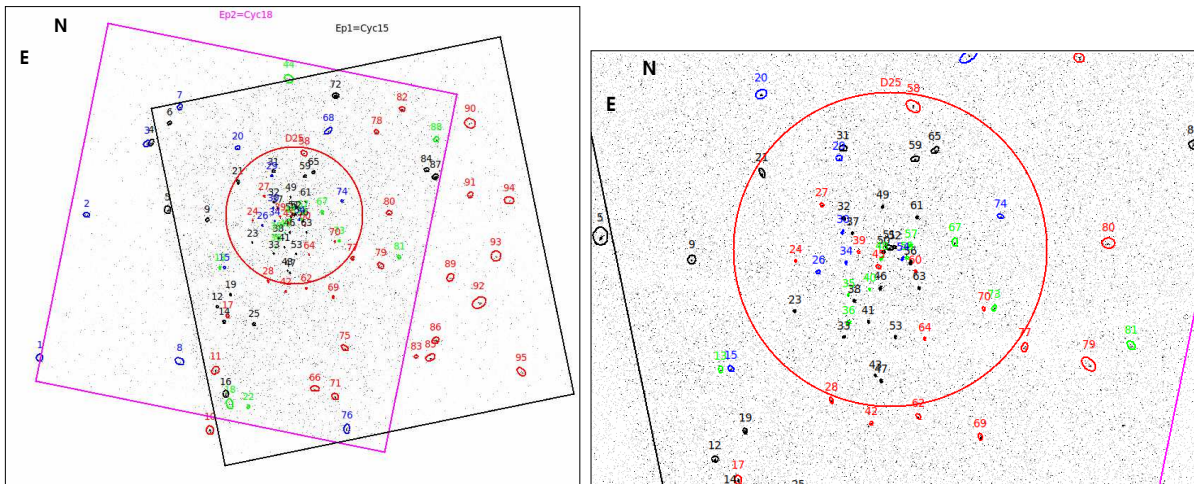
⁵ Berkeley-Illinois-Maryland Array, Thornley (2004)

⁶ <https://ned.ipac.caltech.edu>

Table 1. Basic Properties of NGC 3938

Quantity	Value
Position: RA, Dec	11:52:49.4, +44:07:14.6 (NED)
Distance	22 Mpc (see §1 and §8)
Column Density	$1.77 \times 10^{20} \text{ cm}^{-2}$ (HI4PI; Bekhti et al. (2016))
D25 radius	190.3'' (NED)
<i>Chandra</i> exposures	obsID 15389, 49.3 ksec = Epoch 1 obsID 18456, 45.5 ksec = Epoch 2
Pointing center	11:52:46.1, +44:05:26.4 (Ep1) 11:52:59.8, +44:06:38.4 (Ep2)

Figure 1. Field-of-view from *Chandra* for NGC 3938 with detected sources identified. Each observation was made using ACIS-I, so the field-of-view of the four CCDs is $\sim 16'$ on a side. (left) sources outside the D25 circle; (right) expanded view of the sources inside of the D25 circle. The image scale is set by the D25 radius of $\sim 190''$. North is up and East is left for both images. Ellipses are determined (size, orientation) by the source detection algorithm (§2.1); ellipse colors are defined in Figure 2 (to better see their meaning), refer to the observation epochs, and are used throughout the paper.



2. OBSERVATIONS AND DATA REDUCTION

2.1. *Chandra* Observations

NGC 3938 was the target of two pointed observations made with the Advanced Charge-Coupled Device (CCD) Imaging Spectrometer (ACIS) (Garmire et al. 2003) aboard *Chandra* (Weisskopf et al. 2002): both of these observations were guaranteed time to G. Garmire (Pennsylvania State University). The first observation occurred on 2013 June 28 (ObsID 15389) and the second occurred on 2016 Oct 1 (ObsID 18456): the exposure times of these observations were 40 ksec and 45 ksec, respectively. The aim point for both observations was off the nucleus: the first by ~ 2.7 arcmin SSW and the second by ~ 1 arcmin SSE. In both cases, the entire galaxy was covered essentially by the I3 CCD. Both observations were obtained using the front-illuminated I0-I3 CCDs in Very Faint mode. After correcting for the deadtime, the two exposures were 49.3 and 45.5 ksec. Table 1 lists some basic properties of NGC 3938 and the *Chandra* observations. Figure 1 shows the detected sources (described next) overlaid on the *Chandra* images. Figure 2 overlays the *Chandra* sources on IRAC 3.6μ and Digital Sky Survey 2 blue images of NGC 3938.

The *Chandra* Interactive Analysis of Observations (CIAO) software (version 4.13) and the associated calibration files (version 4.10.3) were used (Fruscione et al. 2006). We accumulated source-free background areas away from the galaxy – broadly described as originating in the corners of the CCDs. We extracted a light curve using 50-second bins to test for the presence of soft background flares; no flares were detected.

Figure 2. (left) Detected X-ray sources within the D25 radius (red circle) overlaid on an IRAC $3.6\mu\text{m}$ image (left) of NGC 3938 and on a SDSS g (DR7) image (right). North is up and East is left. A $1'$ scale bar is in the lower left corner of both images. As stated previously, the ellipses are determined by the source detection routine. Colors are assigned as follows: black (or white/yellow if a dark background): detected source is present in both epochs; red: present only in Epoch 1; blue: only present in Epoch 2; green: only present in the merged data. This color coding is used whenever X-ray detections are overlaid on an image of NGC 3938.

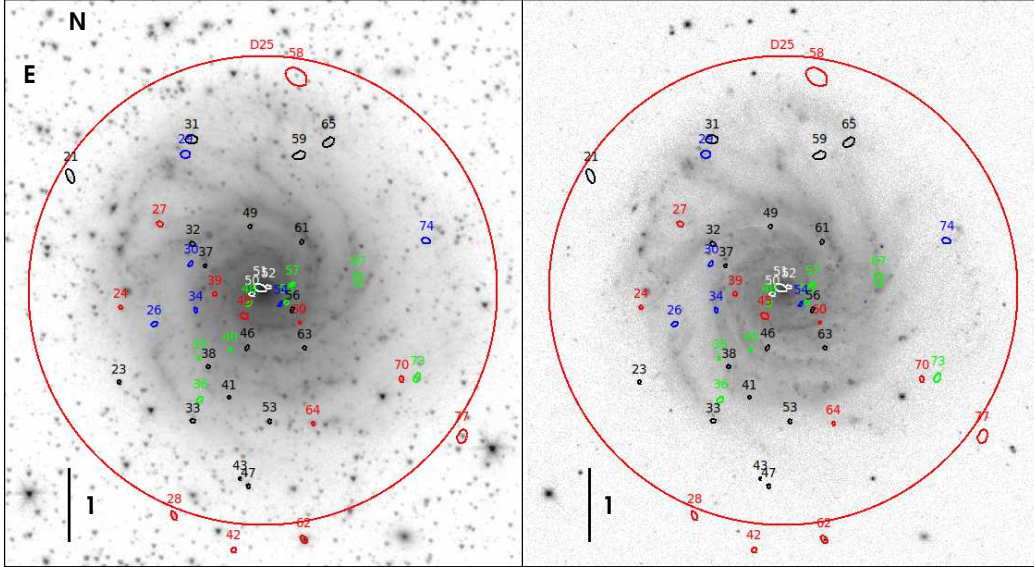


Table 2. Number of Detected Sources by Epoch, Band, and Position

Data set	B	S	M	H	<D25	>D25
Epoch 1	66	14	57	45	33	33
Epoch 2	48	2	37	34	27	21
merged	95	19	44	70	47	48

The epoch data were merged using CIAO task `merge_obs` that yielded a single data set with an exposure time of ~ 94 ksec. The source detection routine `wavdetect` was run on each epoch individually, on the merged data set, and on four bands: B = Broad: 0.3-8 keV; S = Soft: 0.3-1.0 keV; M = Medium: 1.0-2.0 keV; H = Hard: 2-8 keV (Figure 1)⁷.

Point sources were detected using `wavdetect` at $1''$, $2''$, $4''$ and $8''$ scales (Freeman et al. 2002) using the recommended 10^{-6} false-source threshold (1 false source per CCD). The X-ray background for each source was determined from merging ‘blank-sky’ images from the *Chandra* archive and re-projecting the merged data to the position of NGC 3938. For each detected source a corresponding region of the merged blank sky was extracted to determine the background counts. The reader should also note that we do not consider variability at this stage – a variable source could lie above our detection threshold for a limited portion of the observation, but over the entire observation it falls below our threshold.

The detected sources were merged into a final source list after eliminating duplicate detections. Source and background counts were extracted by `wavdetect` using apertures centered on the `wavdetect` positions and of sufficient radius to enclose 95% of the detected X-rays. The J2000 epoch is used for any and all positions throughout this paper. We also checked the astrometry for sources in common between *Chandra* and *GAIA* and *Hubble* and *GAIA*. Positional differences were less than ~ 0.08 arcsec.

Table 2 displays the numbers of detected sources both merged, by band, and by observation epoch. Sources in the broad band were counted as detected if the statistical significance was $>3\sigma$. Sources in the sub-bands were also counted with that significance. Sources in the broad band were matched into the sub-bands regardless of the statistical

⁷ The words Broad, Soft, Medium, and Hard will be used throughout the paper in place of the energy ranges.

Table 3. NGC 3938: Merged Source List: Descending RA Order

N	RA	Dec	Counts	Unc	BkgCts	BkUnc	SrcRate	SrcRUnc	BkgRate	BkRUnc	Signif	Epoch ^a	Cntrpt
Within the D25 Circle													
21	11:53:03.92	44:08:47.04	45.6	7.48	10.4	0.07	4.79e-04	7.86e-05	1.09e-04	7.55e-07	10.5	1,2	
23	11:53:00.25	44:06:00.11	136.7	11.87	4.3	0.05	1.44e-03	1.25e-04	4.54e-05	4.76e-07	42.0	1,2	
24	11:53:00.13	44:07:00.77	25.3	5.29	2.7	0.04	2.66e-04	5.56e-05	2.80e-05	3.75e-07	8.9	1	IR?
26	11:52:57.59	44:06:47.27	12.0	3.87	3.0	0.04	1.26e-04	4.07e-05	3.15e-05	3.88e-07	4.1	2	
27	11:52:57.17	44:08:08.38	65.5	8.43	5.5	0.05	6.88e-04	8.85e-05	5.74e-05	5.28e-07	18.8	1	
28	11:52:56.10	44:04:11.97	17.2	4.58	3.8	0.04	1.80e-04	4.81e-05	4.01e-05	4.46e-07	5.5	1	
29	11:52:55.24	44:09:04.97	15.2	4.58	5.8	0.05	1.60e-04	4.81e-05	6.10e-05	5.67e-07	4.3	2	
30	11:52:54.85	44:07:35.93	13.4	4.00	2.6	0.03	1.41e-04	4.20e-05	2.75e-05	3.66e-07	4.7	2	
31	11:52:54.79	44:09:16.98	19.4	5.29	8.6	0.07	2.04e-04	5.56e-05	9.02e-05	6.87e-07	4.8	1,2	
32	11:52:54.71	44:07:52.04	163.3	13.04	6.7	0.06	1.72e-03	1.37e-04	7.03e-05	5.97e-07	43.8	1,2	
33	11:52:54.69	44:05:28.88	39.9	6.56	3.1	0.04	4.19e-04	6.89e-05	3.25e-05	4.00e-07	13.5	1,2	HII? IR?
34	11:52:54.46	44:06:58.43	15.4	4.24	2.6	0.03	1.62e-04	4.46e-05	2.75e-05	3.66e-07	5.4	2	
35	11:52:54.22	44:06:19.57	8.4	3.16	1.6	0.03	8.80e-05	3.32e-05	1.70e-05	2.91e-07	3.3	mrgd	
36	11:52:54.16	44:05:45.85	9.8	3.61	3.2	0.04	1.03e-04	3.79e-05	3.35e-05	4.08e-07	3.3	mrgd	
37	11:52:53.74	44:07:34.48	40.0	6.63	4.0	0.04	4.20e-04	6.97e-05	4.20e-05	4.58e-07	12.6	1,2	IR?
38	11:52:53.51	44:06:12.51	70.2	8.60	3.8	0.04	7.38e-04	9.03e-05	3.96e-05	4.41e-07	22.5	1,2	
39	11:52:53.03	44:07:11.47	25.6	5.39	3.4	0.04	2.69e-04	5.66e-05	3.58e-05	4.26e-07	8.4	1	
40	11:52:51.84	44:06:26.45	11.9	3.74	2.1	0.03	1.25e-04	3.93e-05	2.17e-05	3.29e-07	4.5	mrgd	
41	11:52:51.94	44:05:47.59	89.5	9.64	3.5	0.04	9.40e-04	1.01e-04	3.67e-05	4.27e-07	29.3	1,2	IR?
42	11:52:51.60	44:03:44.10	22.3	5.10	3.7	0.04	2.34e-04	5.36e-05	3.91e-05	4.44e-07	7.2	1	
43	11:52:51.15	44:04:42.17	48.6	7.28	4.4	0.05	5.11e-04	7.65e-05	4.57e-05	4.77e-07	14.9	1,2	IR?
45	11:52:50.79	44:06:53.63	14.2	4.36	4.8	0.05	1.50e-04	4.58e-05	5.00e-05	4.95e-07	4.3	1	HII?
46	11:52:50.59	44:06:27.83	27.7	5.57	3.3	0.04	2.90e-04	5.85e-05	3.51e-05	4.17e-07	9.1	1,2	
47	11:52:50.52	44:04:35.93	185.5	13.86	6.5	0.06	1.95e-03	1.46e-04	6.84e-05	5.85e-07	50.2	1,2	
48	11:52:50.46	44:07:03.76	12.7	4.00	3.3	0.04	1.33e-04	4.20e-05	3.50e-05	4.15e-07	4.2	mrgd	
49	11:52:50.36	44:08:06.29	167.2	13.19	6.8	0.06	1.76e-03	1.39e-04	7.19e-05	6.03e-07	44.5	1,2	
50	11:52:50.23	44:07:11.41	53.0	7.68	6.0	0.05	5.57e-04	8.07e-05	6.25e-05	5.70e-07	14.8	1,2	
51	11:52:49.59	44:07:16.56	57.9	8.31	11.1	0.07	6.08e-04	8.72e-05	1.17e-04	7.73e-07	13.0	1,2	
52	11:52:49.00	44:07:17.52	28.6	5.74	4.4	0.05	3.00e-04	6.03e-05	4.66e-05	4.86e-07	8.7	1,2	
53	11:52:48.91	44:05:28.55	36.4	6.32	3.6	0.04	3.83e-04	6.64e-05	3.74e-05	4.29e-07	11.8	1,2	IR?
54	11:52:48.09	44:07:03.51	14.0	4.24	4.0	0.04	1.47e-04	4.46e-05	4.20e-05	4.52e-07	4.4	2	
55	11:52:47.62	44:07:04.56	8.9	3.46	3.1	0.04	9.32e-05	3.64e-05	3.28e-05	4.13e-07	3.0	mrgd	
56	11:52:47.19	44:06:58.76	22.6	5.10	3.4	0.04	2.37e-04	5.36e-05	3.57e-05	4.26e-07	7.4	1,2	
57	11:52:47.17	44:07:19.48	9.5	3.46	2.5	0.03	9.99e-05	3.64e-05	2.61e-05	3.59e-07	3.4	mrgd	
58	11:52:46.89	44:10:07.67	23.8	6.56	19.2	0.11	2.50e-04	6.89e-05	2.02e-04	1.13e-06	4.3	1	
59	11:52:46.67	44:09:04.11	25.7	5.92	9.3	0.07	2.70e-04	6.21e-05	9.79e-05	7.15e-07	6.2	1,2	
60	11:52:46.65	44:06:48.46	363.2	19.26	7.8	0.06	3.81e-03	2.02e-04	8.24e-05	6.35e-07	92.4	1	
61	11:52:46.48	44:07:53.67	104.2	10.49	5.8	0.05	1.09e-03	1.10e-04	6.09e-05	5.52e-07	29.3	1,2	HII?
62	11:52:46.32	44:03:52.55	16.3	4.69	5.7	0.05	1.71e-04	4.93e-05	5.99e-05	5.56e-07	4.6	1	
63	11:52:46.25	44:06:27.85	145.8	12.25	4.2	0.04	1.53e-03	1.29e-04	4.43e-05	4.71e-07	45.2	1,2	
64	11:52:45.63	44:05:26.79	16.9	4.36	2.1	0.03	1.78e-04	4.58e-05	2.20e-05	3.34e-07	6.3	1	
65	11:52:44.45	44:09:14.60	45.3	7.48	10.7	0.07	4.76e-04	7.86e-05	1.12e-04	7.65e-07	10.3	1,2	
67	11:52:42.22	44:07:23.77	17.0	5.00	8.0	0.06	1.79e-04	5.25e-05	8.40e-05	6.68e-07	4.3	mrgd	
70	11:52:38.96	44:06:02.52	23.1	5.29	4.9	0.05	2.43e-04	5.56e-05	5.15e-05	5.21e-07	6.8	1	IR?
73	11:52:37.80	44:06:03.89	10.5	4.00	5.5	0.05	1.11e-04	4.20e-05	5.73e-05	5.44e-07	3.0	mrgd	
74	11:52:37.09	44:07:54.61	11.4	4.24	6.6	0.06	1.20e-04	4.46e-05	6.93e-05	6.09e-07	3.1	2	
77	11:52:34.40	44:05:16.25	17.2	4.80	5.8	0.05	1.81e-04	5.04e-05	6.05e-05	5.51e-07	4.9	2	

Notes: ^a Epoch: sources are listed as '1' or '2' from detection in Epoch 1 or Epoch 2, respectively. 'mrgd' means that the source was detected *only* in the merged data.

That does not preclude it from being present in Epochs 1 or 2, but such sources did not exceed the statistical cutoff.
Table heading abbreviations: 'Unc' = UNCertainty; 'BkgCts' = BackGound CounTS; 'BkUnc' = BackGground count UNCertainty; 'SrcRate' = SourCe count RATE; 'SrcRUnc' = SourCe Rate UNCertainty; 'BkgRate' = BackGground RATE; 'BkRUnc' = BackGground Rate UNCertainty; 'Signif' = statistical SIGNificance; 'Cntrpt' = Counterpart (see §2.3; Inside D25).

significance in the sub-band. This approach permitted extracting color information about each detected source even when some of the color information led to upper limits.

All detected sources were also compared to the limiting *count* sensitivity of the CCDs as determined by the CIAO routine `lim_sens`. The limiting sensitivity task convolves the exposure map across the field-of-view with the effective area that any given X-ray would sense. Consequently, sources well off the optical axis must necessarily be brighter to be detected. Such sources all fell below 10 counts. Detections with extracted counts fewer than the limiting sensitivity value at the location of the detected source were dropped. That limit is also the point at which the source count distributions of the *ChaMP* project peaked (their Figure 16; Kim et al. 2007). We followed the limiting sensitivity values across the field-of-view. However, for NGC 3938, the field-of-view of ACIS-I is sufficiently large and the galaxy sufficiently distant and small that sources near the edge of the *galaxy* are essentially unaffected by the limiting sensitivity map. This is our primary motivation for splitting the detected sources into 'inside' and 'outside' the D25 circle. Table 3 lists *all* detected sources in descending Right Ascension order and further separated into 'inside' and 'outside' the D25 circle. The sources *outside* the D25 circle are described in the Appendix for organization sake.

The merged, detected sources were *numbered* in descending Right Ascension (RA) order regardless of their position within the ACIS field-of-view. The merged source list was then separated into 'inside' and 'outside' the D25 circle as

Table 3. NGC 3938: Merged Source List (continued)

N	RA	Dec	Counts	Unc	BkgCts	BkUnc	SrcRate	SrcRUnc	BkgRate	BkRUnc	Signif	Epoch ^a	Cntrprt
Outside the D25 Circle													
1	11:53:54.95	44:00:39.37	17.9	5.57	13.1	0.09	1.88e-04	5.85e-05	1.38e-04	9.69e-07	3.8	2	(2)
2	11:53:42.95	44:07:15.76	42.9	7.94	20.1	0.11	4.50e-04	8.34e-05	2.11e-04	1.19e-06	7.7	2	star
3	11:53:27.49	44:10:33.65	22.7	6.25	16.3	0.10	2.38e-04	6.56e-05	1.72e-04	1.07e-06	4.4	2	(2)
4	11:53:26.38	44:10:35.92	25.9	7.07	24.1	0.12	2.72e-04	7.43e-05	2.53e-04	1.30e-06	4.3	1,2	galaxy
5	11:53:22.11	44:07:30.51	78.4	10.68	35.6	0.15	8.23e-04	1.12e-04	3.74e-04	1.57e-06	11.1	1,2	star
6	11:53:21.60	44:11:31.22	78.2	11.66	57.8	0.19	8.21e-04	1.22e-04	6.07e-04	2.01e-06	9.0	1,2	IR src
7	11:53:18.95	44:12:15.47	31.3	7.35	22.7	0.12	3.28e-04	7.72e-05	2.39e-04	1.26e-06	5.3	2	galaxy
8	11:53:18.94	44:00:30.10	22.1	6.17	15.9	0.10	2.32e-04	6.48e-05	1.67e-04	1.05e-06	4.4	2	(3?)
9	11:53:11.83	44:07:02.15	36.5	7.07	13.5	0.08	3.83e-04	7.43e-05	1.42e-04	8.61e-07	7.6	1,2	galaxy
10	11:53:11.11	43:57:19.53	72.9	9.85	24.1	0.12	7.65e-04	1.03e-04	2.53e-04	1.31e-06	12.2	1	(2?)
11	11:53:09.72	44:00:05.07	49.8	9.22	35.2	0.15	5.23e-04	9.68e-05	3.70e-04	1.57e-06	7.1	1	(3?)
12	11:53:09.19	44:03:00.93	31.2	6.32	8.8	0.07	3.28e-04	6.64e-05	9.20e-05	6.92e-07	7.6	1,2	(1)
13	11:53:08.57	44:04:49.19	10.1	3.87	4.9	0.05	1.06e-04	4.07e-05	5.15e-05	5.22e-07	3.0	mrkd	galaxy
14	11:53:07.46	44:02:19.35	119.7	12.17	28.3	0.13	1.26e-03	1.28e-04	2.97e-04	1.39e-06	18.8	1,2	QSO
15	11:53:07.40	44:04:50.38	16.4	4.90	7.6	0.06	1.72e-04	5.15e-05	7.98e-05	6.43e-07	4.2	2	no cntrprt??
16	11:53:07.01	43:58:59.61	53.8	9.27	32.2	0.14	5.65e-04	9.74e-05	3.38e-04	1.49e-06	8.0	1,2	star
17	11:53:06.57	44:02:35.85	40.0	7.00	9.0	0.07	4.20e-04	7.35e-05	9.48e-05	7.27e-07	9.7	1	galaxy
18	11:53:06.03	43:58:32.44	24.4	7.62	33.6	0.14	2.56e-04	8.00e-05	3.53e-04	1.52e-06	3.6	mrkd	galaxy
19	11:53:05.80	44:03:34.85	116.7	11.18	8.3	0.06	1.23e-03	1.17e-04	8.68e-05	6.77e-07	29.2	1,2	galaxy
20	11:53:04.01	44:10:22.41	29.9	7.00	19.1	0.11	3.14e-04	7.35e-05	2.00e-04	1.14e-06	5.5	2	IR src
22	11:53:01.18	43:58:23.28	29.5	7.94	33.5	0.15	3.10e-04	8.34e-05	3.52e-04	1.53e-06	4.3	mrkd	galaxy
25	11:52:59.80	44:02:13.48	38.1	6.93	9.9	0.07	4.01e-04	7.28e-05	1.04e-04	7.36e-07	9.0	1,2	galaxy
44	11:52:50.79	44:13:33.43	27.4	7.62	30.6	0.14	2.87e-04	8.00e-05	3.22e-04	1.45e-06	4.1	mrkd	IR src
66	11:52:44.06	43:59:14.79	20.0	6.78	26.0	0.13	2.10e-04	7.12e-05	2.73e-04	1.34e-06	3.2	1	galaxy
68	11:52:40.63	44:11:09.48	24.9	7.07	25.1	0.13	2.62e-04	7.43e-05	2.64e-04	1.31e-06	4.1	2	(3?)
69	11:52:39.36	44:03:28.05	37.4	6.71	7.6	0.06	3.93e-04	7.05e-05	7.97e-05	6.43e-07	9.6	1	IR src
71	11:52:38.90	43:58:52.62	41.8	8.66	33.2	0.14	4.39e-04	9.10e-05	3.49e-04	1.51e-06	6.1	1	galaxy
72	11:52:38.72	44:12:47.03	612.8	26.59	94.2	0.25	6.44e-03	2.79e-04	9.89e-04	2.61e-06	57.0	1,2	galaxy
75	11:52:36.43	44:01:07.52	22.3	6.40	18.7	0.11	2.34e-04	6.73e-05	1.97e-04	1.13e-06	4.1	1	IR src
76	11:52:35.95	43:57:23.44	37.4	8.89	41.6	0.16	3.93e-04	9.34e-05	4.37e-04	1.70e-06	5.0	2	(1 ft)
78	11:52:28.20	44:11:06.12	35.8	8.60	38.2	0.15	3.75e-04	9.04e-05	4.02e-04	1.62e-06	4.9	1	(3?)
79	11:52:27.17	44:04:55.72	27.2	6.71	17.8	0.11	2.86e-04	7.05e-05	1.87e-04	1.10e-06	5.1	1	(1?)
80	11:52:24.95	44:07:22.06	43.1	9.59	48.9	0.18	4.53e-04	1.01e-04	5.13e-04	1.84e-06	5.4	1	(1 br, 2 ft)
81	11:52:22.39	44:05:18.34	20.3	6.56	22.7	0.12	2.13e-04	6.89e-05	2.38e-04	1.25e-06	3.5	mrkd	(1)
82	11:52:21.55	44:12:09.61	51.7	10.05	49.3	0.18	5.43e-04	1.06e-04	5.18e-04	1.85e-06	6.4	1	(1)
83	11:52:18.05	44:00:42.85	26.1	6.71	18.9	0.11	2.74e-04	7.05e-05	1.99e-04	1.14e-06	4.8	1	(1)
84	11:52:15.28	44:09:21.04	43.7	8.95	36.3	0.15	4.59e-04	9.40e-05	3.81e-04	1.58e-06	6.2	1,2	star
85	11:52:14.41	44:00:40.71	47.5	8.37	22.5	0.12	4.99e-04	8.79e-05	2.37e-04	1.25e-06	8.1	1	(3)
86	11:52:13.09	44:01:28.32	62.8	9.27	23.2	0.12	6.59e-04	9.74e-05	2.44e-04	1.27e-06	10.6	1	IR src
87	11:52:13.07	44:09:01.97	155.5	15.84	95.5	0.25	1.63e-03	1.66e-04	1.00e-03	2.59e-06	14.4	1,2	radio src
88	11:52:12.80	44:10:45.61	35.4	8.55	37.6	0.15	3.72e-04	8.97e-05	3.95e-04	1.62e-06	4.9	mrkd	(2?)
89	11:52:09.23	44:04:22.41	29.5	6.86	17.5	0.10	3.10e-04	7.20e-05	1.83e-04	1.10e-06	5.6	1	(4?)
90	11:52:04.10	44:08:11.45	26.5	7.14	24.5	0.12	2.78e-04	7.50e-05	2.58e-04	1.31e-06	4.4	1	(1 star?)
91	11:52:04.05	44:11:29.82	45.8	9.44	43.2	0.17	4.81e-04	9.91e-05	4.54e-04	1.74e-06	6.0	1	galaxy
92	11:52:01.84	44:03:12.23	87.6	12.57	70.4	0.21	9.20e-04	1.32e-04	7.39e-04	2.22e-06	9.3	1	(1 br, 6 ft)
93	11:51:57.46	44:05:21.37	40.0	8.78	37.0	0.15	4.20e-04	9.22e-05	3.89e-04	1.61e-06	5.6	1	star
94	11:51:54.02	44:07:55.79	23.7	7.00	25.3	0.13	2.49e-04	7.35e-05	2.65e-04	1.33e-06	3.9	1	(2)
95	11:51:51.00	43:59:59.95	32.3	7.75	27.7	0.13	3.39e-04	8.14e-05	2.91e-04	1.41e-06	5.1	1	(3?)

Notes: See the Appendix for a description of the objects in this >D25 table. ^a Epoch: sources are listed as '1' or '2' from detection in Epoch 1 or Epoch 2, respectively. 'mrkd' means that the source was detected *only* in the merged data. That does not preclude it from being present in Epochs 1 or 2, but such sources did not exceed the statistical cutoff. Under 'Cntrprts': numbers in () indicate potential counterparts visible in *Spitzer* IRAC data. 'br' = bright; 'ft' = faint.

mentioned above (Table 3). The detected source tables for Epochs 1 and 2 are contained in the Appendix and follow the same numbering approach. We count 47 sources within or on the D25 circle: sources 21, 23, 24, 26 to 43, 45 to 65, 67, 70, 73, 74, and 77. All other detected objects lie outside of the D25 circle.

2.2. Detected Sources versus the Chandra Source Catalog

We must address differences between our detected source list and the list from the Chandra Source Catalog (Evans et al. 2010) (hereafter, CSC). We here focus on the source differences within the D25 circle and leave the sources outside the D25 circle to Appendix A.

There are 36 sources in common between the two source lists. However, there are six sources detected within D25 on the CSC list that are not on our list and five sources on our list that are not in the CSC. For both source lists, the detected objects are essentially all on axis or sufficiently close that changes with off-axis angle are not at all important.

The detected source list differences could fall into two reasonable categories: below our minimum signal-to-noise value or only detected from the merged Epoch 1 and Epoch 2 data sets. There are sources, however, for which we do not have a reasonable explanation. The details follow.

Five of the six CSC sources we fail to detect fall below our minimum signal-to-noise threshold (2CXO J115242.0+440532; 2CXO J115256.7+440902; 2CXO J115258.6+440528; 2CXO J115256.7+440918; 2CXO

115247.1+440434). The sixth one technically would be above our threshold, but the detected events are distributed across a region larger than the PSF (2CXO J115248.5+440704), puzzling for an essentially on-axis source. That may suggest the source is extended – but if it is, it then falls below our detection threshold.

For the five sources on our list not detected by the CSC, we only have an explanation for one: it is on our *merged* list (number 55). The CSC only merges observations if the pointing directions lie within $1'$ of each other. The two observations of NGC 3938 lie $\approx 3'$ apart. The other sources (numbers 26, 29, 30, 34, and 74) all lie above our detection threshold (ranging from ~ 8 to 15 counts). An examination of each shows a small ‘pile’ of events consistent with *Chandra*’s PSF. We consequently do not have an explanation for their lack of detection in the CSC. Source 29 is particularly puzzling as it lies within $\sim 15''$ of a source with a similar count rate that is present on both our and the CSC detected source lists.

2.3. MultiWavelength Source Comparison

One motivation to conduct high angular resolution X-ray observations of nearby spiral galaxies with face-on orientations is the search for counterparts at multiple wavebands to the detected discrete X-ray sources. The ability to see sources in other bands enhances the multi-wavelength connections of types of sources that may not be easily visible in the Milky Way. Consequently, we attempted to correlate detected *Chandra* sources with sources from other bands. We understand that NGC 3938 is sufficiently distant that matching sources is difficult.

Normally, we would separate the very soft sources from the harder sources with the overall assumption that the soft sources are supernova remnants (SNRs). However, given that both epochs of observation of NGC 3938 were obtained relatively late in *Chandra*’s life, the build-up of the contaminant on the ACIS optical blocking window has dramatically reduced the instrument’s effective area sharply for photons with energies of less than 1 keV (below ~ 0.7 - 0.8 keV). This essentially eliminates SNRs as a possible category, particularly for a relatively distant galaxy since SNRs typically produce a majority of their X-ray photons with energies in this range. Furthermore, the limiting luminosity is $\approx 10^{38}$ erg s $^{-1}$, about 10-100 times larger than the typical integrated X-ray luminosity of SNRs (Hamilton & Sarazin (1984); Charles & Seward (1995); Long (2017)). Consequently, we ignore the possibility that any X-ray sources in NGC 3938 are SNRs.

The NED archive also lists a number of H II regions within the D25 circle of NGC 3938. In general, we would not expect H II regions to be X-ray sources, particularly in more distant galaxies, as they are often low-luminosity X-ray-emitting star formation regions ($\sim 10^{33}$ erg s $^{-1}$ e.g., Townsley et al. (2003)) unless powered by a central black hole or some equivalent high-energy source.

We extracted *Spitzer* IRAC sources from the IRAC archive⁸ to learn whether any detected *Chandra* sources matched. The archival data were obtained using the *Spitzer* Space Telescope’s Infrared Array Camera (IRAC – see Fazio et al. (2004)) at 3.6, 4.5, 5.8 and 8.0 μm . Figure 3 shows the images overlaid with *Chandra* detected sources. The sources listed in Table 3 show potentially seven infrared sources matching X-ray positions within the uncertainties (‘IR?’ in the far right column of Table 3). None of the other X-ray sources or infrared sources revealed a matching counterpart.

Figure 4 shows the full range of images of NGC 3938 obtained from summing frames obtained with *Swift*’s UVOT. In comparing the optical with the UV images, one should see that the V band is relatively devoid of specific sources. In contrast, the UV bands exhibit significant emission variations within a spiral arm as the wavelength decreases. That strong UV behavior may mean that high-mass X-ray binaries (HMXBs) could be identified and separated from low-mass XRBs (LMXBs) using the *HST* images (see §3) to build color diagrams from which masses of the main sequence stars in the XRBs are inferred (Chandar et al. 2020). It would be interesting to see the reliability of the approach as a function of distance – to date, this approach has been applied to M83 (Chandar et al. (2020); Hunt et al. (2021)) and M81 (Hunt et al. 2023a) individually and six other galaxies (NGC 628, NGC 3351, NGC 3627, NGC 4321, NGC 4569, and NGC 4826) in a collective study (Hunt et al. 2023b). Either approach, however, lies outside the scope of this paper.

3. SPECIFIC SOURCES – DETECTED OR NOT?

Five supernovae (SNe) have occurred in NGC 3938 over the historical record: SN1961U (RA 11:52:56.81, Dec +44:09:01.1), SN1964L (11:52:49.09, +44:07:45.4), SN 2005ay (11:52:48.07, +44:06:18.4), SN2017ein (11:52:53.25, +44:07:26.20), and SN2022xlp (11:52:49.58, +44:06:03.5). None of the SNe are detected with statistical significance

⁸ ipac.caltech.edu

Figure 3. *Spitzer* images of NGC 3938 in the (left to right) IRAC 3.6, 4.5, 5.8, 8.0, and IRS 24 μm bands. X-ray sources are circled in each band but only identified in the 3.6 μm band. The color coding follows that of Figure 2. X-ray sources do not appear to correlate with any infrared features. North is up, East left. The fields are $\sim 5'$ on a side.

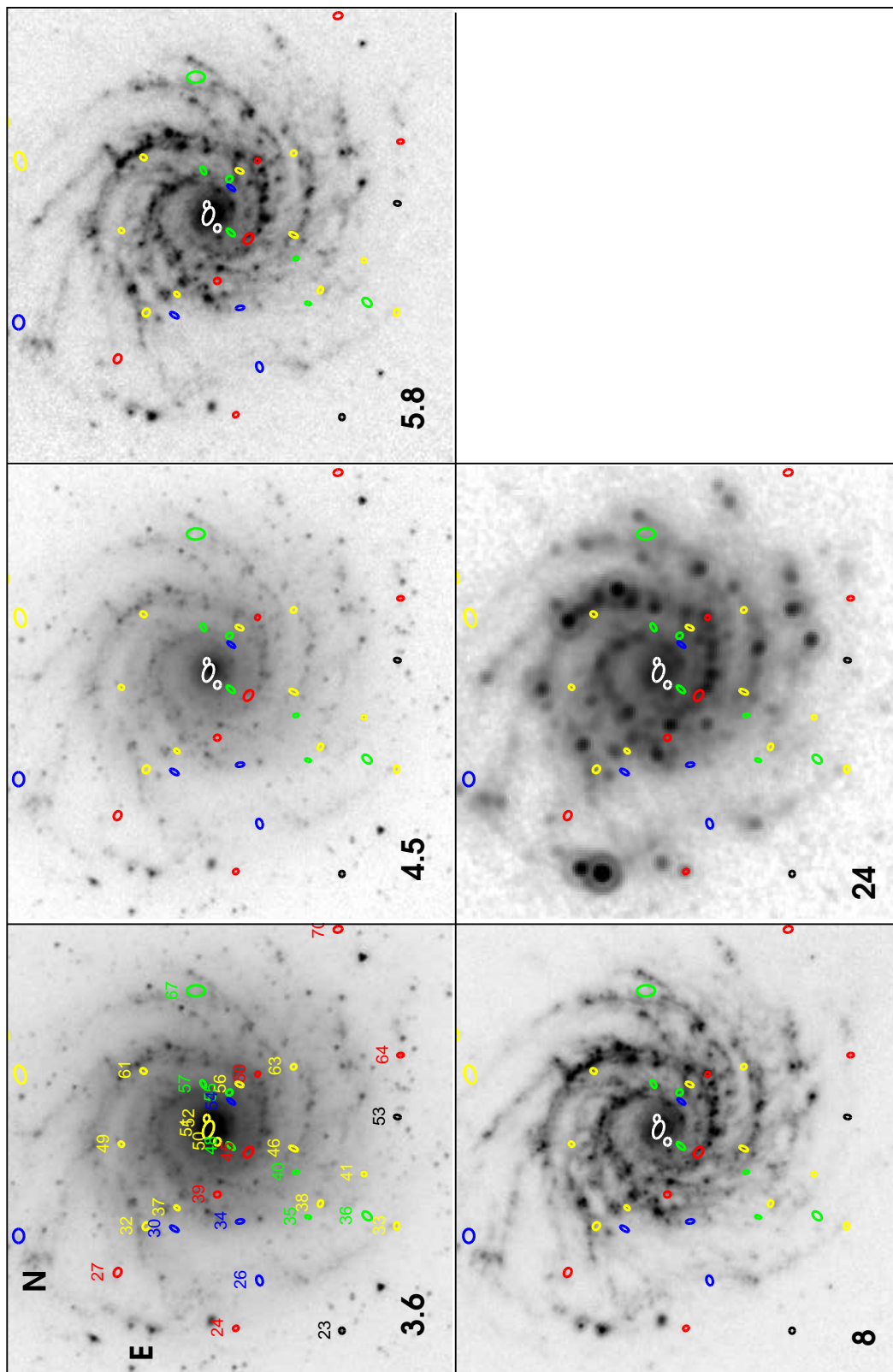


Figure 4. *Swift* UVOT images of NGC 3938 in the (left to right) UW2, UM2, UW1, U, B, and V bands. X-ray sources are circled in each band but only identified in the UW2 band. The color coding is identical to the previous images (Fig. 2). X-ray sources outside of the nucleus but within the D25 circle essentially fall into two groups: on or close to an arm or UV-emitting region, or in a UV-deficient region. North is up, East left. The fields are $\sim 5'$ on a side.

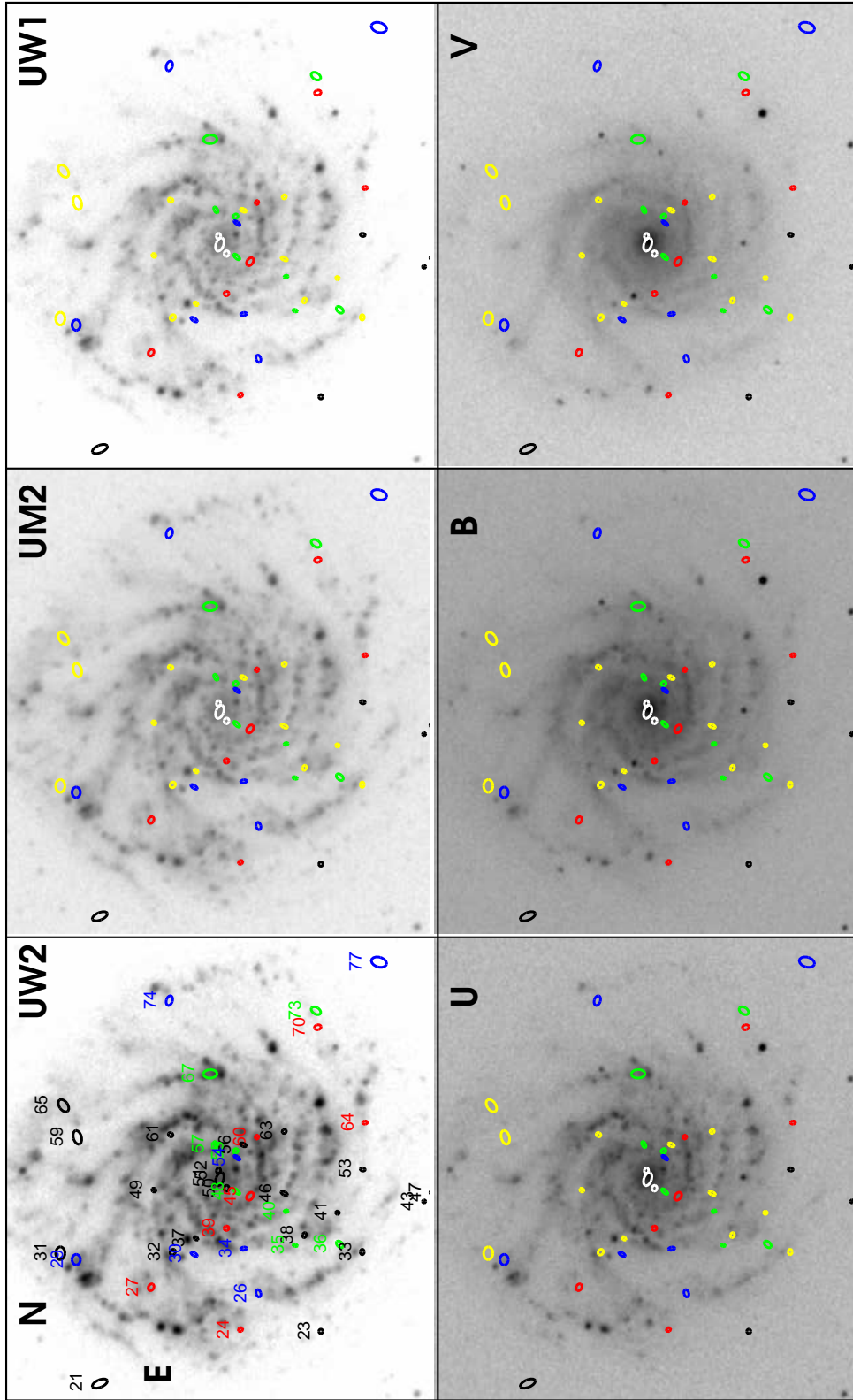
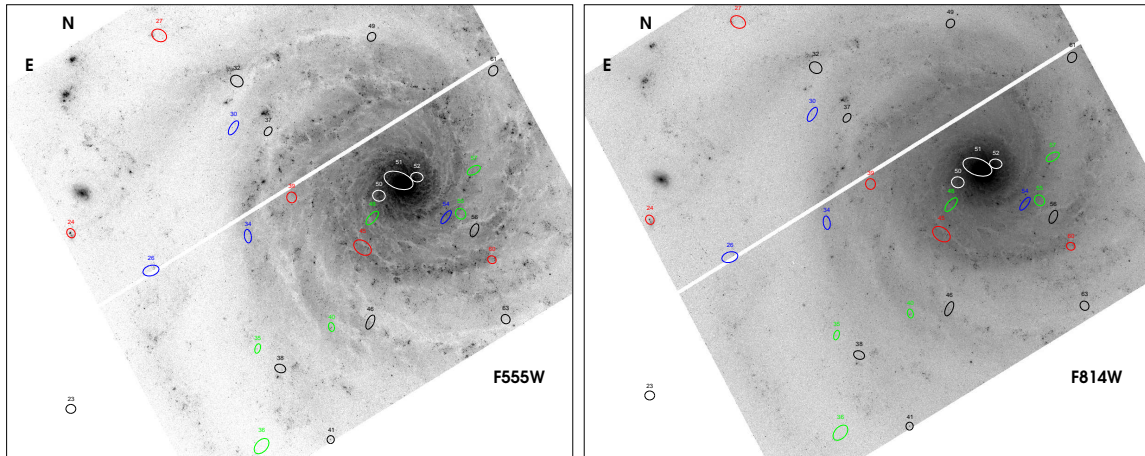


Figure 5. *HST* images (left = F555W; right = F814W) of the nucleus and eastern portions of NGC 3938. X-ray sources are circled in each band. The color coding is identical to that in Figure 2. Note that even at the resolution of *HST*'s WFC instrument and outside of the nucleus only source 24 (near-center left) can be identified to a particular source (q.v. Fig. 6). This significantly contrasts to the situation for sources outside the D25 circle where nearly every source has a known counterpart or a few candidate counterparts (see Table 3). North up, East left. The fields are $\sim 2'$ on a side.



in our analysis. No X-ray-emitting progenitor is found at the position of SN2022xlp nor pre-/post-X-ray emission at the position of SN2017ein.

However, SN1961U and SN1964L reveal a hint of emission – both are detected at $\sim 2 - 2.5 \sigma$ which, properly, is consistent with the background. SN1961U and SN1964L both show detected X-rays – just not enough to merit the ‘significantly detected’ label. The counts are consistent with an X-ray flux upper limit of $\sim 3 \times 10^{37}$ erg s^{-1} . It is quite possible that a future, larger telescope with a PSF at least equivalent to *Chandra* will demonstrate that these objects are X-ray-emitting SNRs. If that is nearly possible with *Chandra* looking at SNRs at ~ 20 Mpc, then future researchers should be able to study many historical SNe in nearby galaxies at relatively early stages of evolution as SNRs.

In addition to SNe, there are two *Hubble* images available for the nucleus and immediate surroundings of NGC 3938 (WFC3 555W and 814W; Figure 5)⁹. One X-ray source matches within 0.2 arcsec with a corresponding optical counterpart in each of the images: source 24. Figure 6 (left) expands the view. The source is not a bright UV source (Fig. 4) but is visible in the IR (Fig. 3). In addition, source 60 matches with a small group of stars (right) but we are unable to pin down a specific candidate.

Finally, we mention the possibility that the nucleus of NGC 3938 is not X-ray bright – perhaps not surprising given its status as a LINER AGN. Figure 7 shows the situation: there appears to be a moderately bright X-ray source $\approx 3''$ to the North (number 51; 36 ± 6.4 and 17.6 ± 4.6 counts in Epochs 1 and 2, respectively), as shown in Figure 7. We immediately considered whether the “known” position of the nucleus is slightly in error. Alternatively, the sources are low-count statistical variations. We deem the first explanation unlikely given the *HST* WFC3 UVIS F555W image that shows a well-defined ‘circulation’ pattern around the nucleus and *centered* on the nucleus using the coordinates as listed in Table 2. Those coordinates were verified in the GAIA reference frame. The Epoch 1 detection list shows a weak, *Soft* source at the nucleus (5.3 ± 2.4 counts equivalent to a 2.4σ detection). No corresponding object exists in the Epoch 2 detection list regardless of the significance.

Furthermore, source 51 is extended E-W, suggesting either that a source is being ripped apart **or an extended ‘cloud’ illuminated by the nucleus** *or* that it is a background extended source *or* that there are multiple sources that are confused at *Chandra*'s resolution. Since NGC 3938's nucleus produces emission $> 5''$ over two epochs of on-axis observations, the possibility that *Chandra* is not resolving the nucleus seems unlikely *if* the ‘source’ is two separate objects. If the ‘source’ is a *string* of X-ray-emitting objects that are blurred together, *Chandra* likely could not resolve them at the distance of NGC 3938. That a background galaxy's light is getting through the nuclear region also seems unlikely. The *HST* image appears uniform in azimuth about the nucleus, supporting the statement that a background galaxy's light could not penetrate the nuclear region. **That leaves a limited set of possibilities: ripped-apart**

⁹ These images were obtained from MAST (MAST 2021) using *HST*.

Figure 6. Expanded view of Sources 24 (left half) and 60 (right half) using the *Hubble* WFC3 images (filters F555W and F814W). The frames are $\sim 8'$ on a side. The color coding matches that of Figure 2.

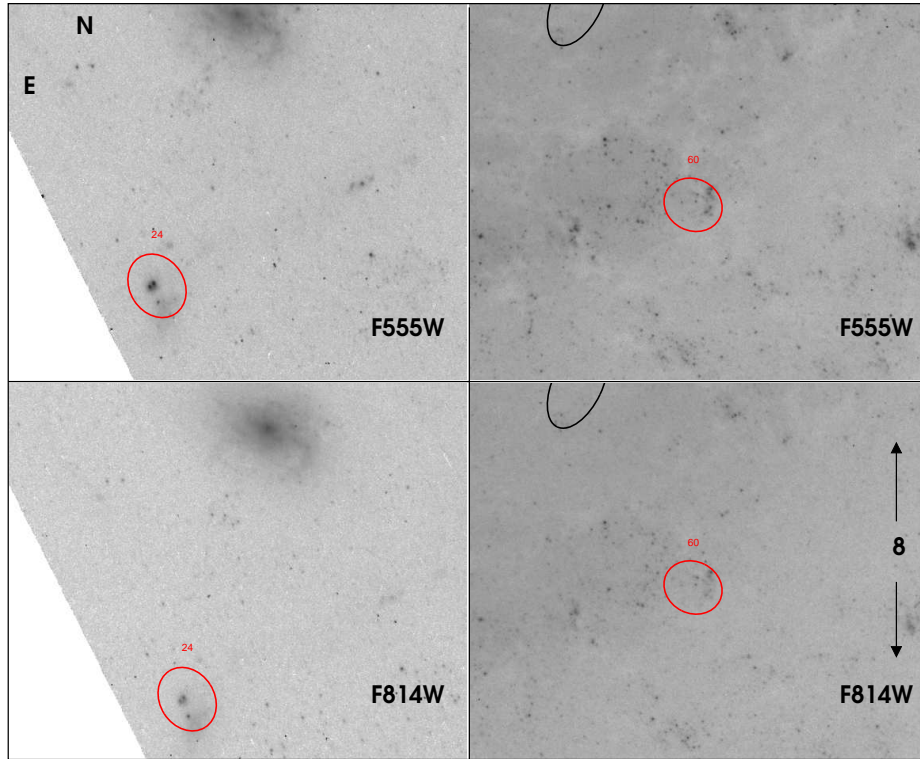
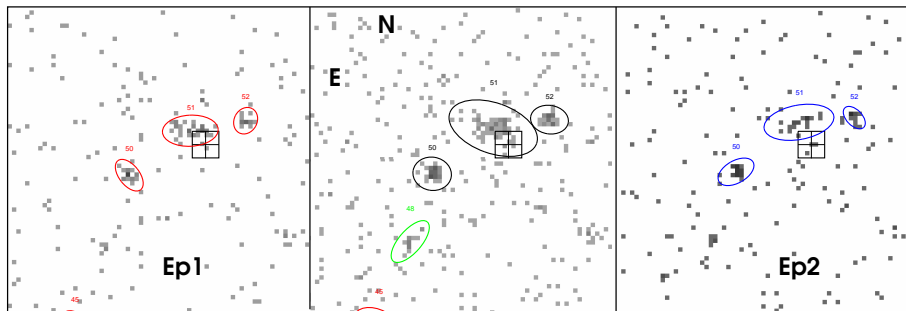


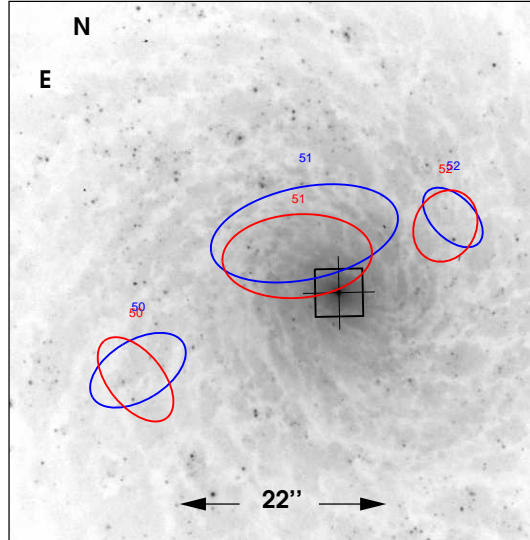
Figure 7. The nuclear region of NGC 3938. From left to right, the nucleus is shown for (left) Epoch 1; (center) the merged data; and (right) Epoch 2. The ellipses are detected sources within the D25 circle of the galaxy. The ellipse for the *merged* data changes orientation slightly likely because the event distribution changes between the two epochs. The box is centered on the nucleus and is $2''$ on a side. The entire field-of-view is $\sim 50''$ on a side. The color coding matches that of Fig. 2.



source or a blurred string of X-ray-emitting objects or something equivalent to an illuminated cloud, for example, the X-ray counterpart of Hanny’s Voorwerp in IC 2497 (Fabbiano & Elvis 2019) or the polarized cloud near Sgr A* (Marin et al. 2023). None of these is an immediately-sensible possibility: a shredded source would likely need to be lit up by the nucleus, but the nucleus is not significantly brighter to do so; a string of X-ray-emitting objects is possible but immediately generates origination questions. An X-ray gas cloud similar to the Voorwerp or Sgr A*’s gas cloud would also appear implausible given the *HST* image. For IC 2497, the X-ray ‘cloud’ lies $\sim 20''$ south of the nucleus, considerably more distant from the nucleus given the ~ 225 Mpc distance to IC 2497. For the Sgr A* cloud, the $\approx 4''$ distance translates to ~ 250 pc at NGC 3938, i.e., ~ 10 times farther or an ~ 100 times lower irradiation. A sufficiently detailed investigation of any of these possibilities lies beyond the scope

of this paper. Clearly the understanding of the nucleus must await a higher-resolution and higher-sensitivity X-ray telescope, e.g., AXIS [Marchesi et al. \(2020\)](#).

Figure 8. The nuclear region of NGC 3938 as observed with the WFC3 UVIS instrument (filter F555W) on *HST*. The ellipses all lie within $\sim 10''$ of the nucleus but are *not* centered on the nucleus. The nucleus lies at the intersection of the cross hairs within the box. The box is $2''$ on a side. The ‘circulation’ is visible in the image. The entire field-of-view is $\sim 22''$ on a side. The color coding matches that of Fig. 2.



4. X-RAY PROPERTIES VIA COLOR-COLOR HARDNESS

[Prestwich et al. \(2003\)](#) describe an X-ray color-color analysis of the discrete sources based on separating each source’s counts into soft, medium, and hard bands. If we follow that approach, defining the bands to be ‘soft’ (S), equal to 0.3-1.0 keV, ‘medium’ (M) as 1.0-2.0 keV, and ‘hard’ (H) as 2.0-8.0 keV which then leads to two colors: M - S and H - M, each normalized by the total counts. The color information is listed in Tables 11 (Epoch 1) and 12 (Epoch 2), both located in the paper’s appendix. The contaminant is expected to alter the positions of the ellipses – we choose to retain the original definitions for comparison with prior publications using this approach.

Figures 9(a) and (b) show the results for NGC 3938 for the individual epochs for sources *within* the D25 circle. We do not present a color-color plot for the merged data because of the optical blocking window build-up.

Of note in both color hardness plots is the complete lack of any sources in the SNR circle, and relatively few in the LMXB circle. As NGC 3938 is a star-forming galaxy, even if at a low rate, it should exhibit some SNRs. Further, given that the galaxy is quite face-on to our perspective, we do not then get to claim ‘excess column density’ within the galaxy as a straightforward explanation even though many of the sources are present in the ‘Absorbed’ circle. The likely explanation at this point, given that both observations were obtained somewhat late in *Chandra*’s lifetime, is the build-up of the absorbing contaminant on the ACIS optical blocking window.

Even for the first epoch of data, that serves to reduce the effective area of the telescope below ~ 1 keV relative to energies above 1 keV. This would preferentially diminish softer sources from detection with little change to medium and harder sources. The question that remains is whether soft sources such as supernova remnants, for example, are present on the detected sources list at all. To address that question will likely require cross-wavelength analyses with pinpointed sources from other bands.

If we assume that much of the ‘motion’ in the Epochs 1 to Soft color occurs because of the contaminant, then that suggests that most of the detected sources in Epoch 1 are LMXBs. That inference then suggests an additional inference: NGC 3938 has not experienced a high star formation rate in the past one-to-a-few Gyrs. If that inference is correct, that inference then goes against the historical presence of five supernovae in this galaxy (§3).

5. SPECTRAL FITS

Figure 9. Color-color plots for each epoch (left) Epoch 1; (right) Epoch 2 for objects *inside* the D25 circle. The left arrow in the Epoch 2 plot indicates the approximate change in each data point solely because of the increase of the optical blocking window absorption between the two epochs. To avoid an unreadable graph, we eliminated uncertainties from some of the data points, leaving a representative sample. For data points without uncertainties, assume the uncertainties are at least as large as those plotted. The ‘powerlaw’ model describes the arc of changes to the colors as the power law index changes (‘dPL’) from its starting point at 3.0. ‘UL’ = Upper Limit. The region ellipses are defined in [Prestwich et al. \(2003\)](#).

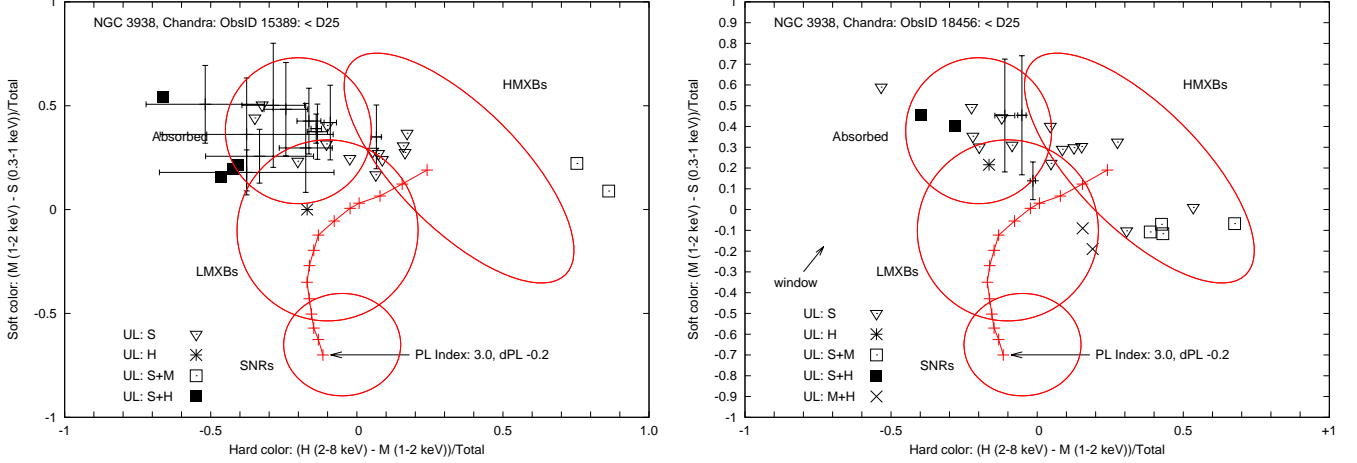


Table 4. Spectral Fit Parameters

SrcN	χ^2 per dof	N_H (10^{22} cm^{-2})	Brems (B, keV) or Powerlaw Index (P)	Calc'd Flux ^a 0.5-2 keV	Calc'd Flux ^a 2-10 keV
60	9.6/15	<2.44	P: 2.52 ± 2.31	3.6(-14)	5.4(-14)
72-1	16.3/12	<0.65	P: 0.88 ± 1.18	4.6(-14)	1.7(-13)
72-2	8.2/13	<0.65	P: 1.27 ± 1.10	4.5(-14)	1.6(-13)
72-2	8.2/13	<0.65	B: <15.7	5.3(-14)	1.2(-13)

^aFluxes calculated using the best-fit model as listed; flux format: n.n(-e) = $n.n \times 10^{-e}$. Uncertainties on each spectral data point were included in the fitting. Uncertainties on the fluxes are not included as the count rate-determined fluxes provide a more statistically-defined value.

There are at best two sources (60 and 72) that are sufficiently bright to warrant the simplest model for spectral fitting. Source 60 lies inside the D25 circle and is only detected in Epoch 1. Source 72 is detected in both observations and lies outside the D25 circle.

We fit the spectra with either an absorbed power law or an absorbed thermal bremsstrahlung spectrum plus a powerlaw for the background. All of the fits returned values with significant uncertainties regardless of the model or fitting approach we adopted. We list the parameter values in Table 4 but do not include any figures of the spectra or parameter contours to save space. The spectra are all peaked around 1 keV, both because of the drop in effective area above that energy and because of the ACIS window build-up below that energy. The result is that the fitted continuum parameters are relatively unconstrained. The background region for these sources is determined by placing a circular region in the portion of *Chandra's* I3 chip without any visible sources, making it as large as possible.

Using our adopted distance of 22 Mpc, source 60 has a 0.5-2 keV flux of $\approx 2 \times 10^{39} \text{ erg s}^{-1}$. If we reduce the adopted distance to 17 Mpc, then the 0.5-2 keV flux drops to $\approx 1.2 \times 10^{39} \text{ erg s}^{-1}$, so still within the ULX definition.

Source 72 lies outside of the D25 circle and corresponds with the galaxy WISEA J114238.74+441247.0. The NED-listed redshift is 0.227 which yields a recession velocity of 68300 km s^{-1} relative to the CMB or a Hubble distance of $\sim 1000 \text{ Mpc}$. At that distance, the observed fluxes are $\sim 6 \times 10^{42}$ and $\sim 2 \times 10^{43} \text{ erg s}^{-1}$ for the 0.5-2 and 2-10 keV bands, respectively. Both values fall above the typical range of normal galaxies and toward the lower end of active galaxies, suggesting a potential LINER or Seyfert AGN based solely on the luminosity values.

6. TIMING

There are two time frames to be described: (i) variations *within* an observation; and (ii) variations *between* the two epochs. First, the variations within an observation and within the D25 radius (sources outside D25 were also analyzed – see the appendix.) were analyzed using the CIAO.glvary routine (Gregory & Loredo 1992). This makes use of the aspect solution to project the effective area at a given source’s location so to account for pixel-to-pixel sensitivity changes as well as effective area changes caused by chip edges. The CIAO prescription for *glvary*¹⁰, as described in the science thread, was followed.

For the first epoch, no sources within the D25 circle (and only one source outside) were estimated to have a variability index of 2 or more¹¹.

For the second epoch, only one source (77) had a variability index of 2 or more. However, the source has two arguments against interpreting it as a variable object: there were a total of ~ 17 detected counts and the object was positioned in a gap between ACIS CCDS I3 and I1. The presence of the source in the gap will almost certainly introduce a variation in the detected count rate, even given the Lissajous pattern *Chandra* uses to avoid sources falling permanently between chip gaps. We do not conclude that the source varies.

The variations *between* observations were analyzed with a different approach. For this problem, we are not interested in small-scale changes, but in the total counts (or count rate) between the two epochs. Given that the aim-points of the two epoch were within 3.2’ of each other, and given the approximately symmetric behavior of ACIS-I about the aimpoint, then the off-axis sources would approximately experience the same off-axis behavior. That means we can compare the total counts for each source between the two epochs to a reasonable accuracy.

The one item that must be addressed between the two epochs is the increasing absorption accumulating on the ACIS optical blocking window. We used the CIAO proposal tool to calculate, for adopted *bremsstrahlung* spectra of 1, 5, and 10 keV, the expected counts of Epoch 2 (Cycle 18) targets given Epoch 1 (Cycle 15) count rates. This led to a ‘correction’ factor to increase Epoch 2 counts for comparison with the Epoch 1 counts. The correction factor varied minimally for different temperatures of the adopted spectrum. We adopted an Epoch 2 / Epoch 1 correction factor of 1.23 to be applied to the Epoch 2 source counts. We ignore all sources that are only detected in the merged data as well as sources that were not consistently on the CCDs across both epochs.

With that correction factor in hand, we then generated Table 5 which lists the combined sources detected in Epochs 1 and 2, with their Epochs 1 and 2 counts, the corrected Epoch 2 counts, and a label describing whether a comparison of the Epoch 1 and corrected Epoch 2 counts were constant or varied within 3 standard deviations. With those requirements, five sources meet the ‘variable’ criterion: two are on the boundary between constant and variable, while three are well beyond the ‘constant’ criterion. We caution the reader that the window build-up introduces additional uncertainty that only more timing data would address.

Finally, there are those sources that were not detected in both epochs. Sources within the D25 circle were within the fields-of-view of the ACIS detector. Furthermore, sources within the D25 circle fell within the relatively flat ‘unit response’ of the ACIS CCDs. Consequently, we may infer that these sources underwent a change-of-state between the two observations. Those sources that were detected in Epoch 1 but not in Epoch 2 are: 24, 27, 28, 39, 42, 45, 58, 60, 62, 64, 70, and 77. Those sources detected in Epoch 2 but not in Epoch 1 are: 26, 29, 30, 34, 54, and 74. These results are noted in the rightmost column of Table 3.

In summary, then, NGC 3938 reveals sixteen X-ray sources that were constant between the two observations, five sources detected to be variable, and a further seventeen that were either on, then off or off, then on, between the observations. Consequently, a total of twenty-two sources exhibited variability.

7. STAR FORMATION RATE AND METALLICITY OF NGC 3938

We now present estimates of the star formation rate (SFR) and the metallicity of NGC 3938 based on optical and infrared flux measurements made of the galaxy. We pattern the analysis presented here after the analysis given in our previous work on the galaxy NGC 45 (Pannuti et al. 2015). In the present paper, we implement an updated SFR relation derived by Kennicutt et al. (2009), but we use the same metallicity relation derived by Lee et al. (2006) that we used in Pannuti et al. (2015).

¹⁰ <https://cxc.cfa.harvard.edu/ciao/threads/variable/>

¹¹ An index >2 increasingly raises the probability that the source is variable, starting at a probability of 50%. See the previous footnote for a table linking variability index to probabilities.

Table 5. Variability Between Observation Epochs

SrcN	RA (J2000)	Dec (J2000)	Ep-1 Cts	Ep-1 Unc	Ep-1 Flux	Flux Unc	3sig Unc	Ep-2 Flux	Corr'd Ep2-Fx	Vary? ^a
21	11:53:03.84	44:08:46	33.7	6.93	6.86	1.42	4.26	4.25	5.23	No
23	11:53:00.25	44:06:00	85.4	9.54	17.37	1.07	3.21	14.88	18.30	No
31	11:52:54.73	44:09:16	10.1	3.74	2.06	1.38	4.14	2.73	3.36	No
32	11:52:54.72	44:07:52	87.7	9.64	17.88	1.06	3.18	19.84	24.40	Yes
33	11:52:54.70	44:05:29	25.0	5.20	5.09	1.08	3.24	4.08	5.02	No
37	11:52:53.77	44:07:34	20.0	4.80	4.07	1.15	3.44	5.15	6.33	No
38	11:52:53.51	44:06:12	41.0	6.56	8.32	1.05	3.15	7.61	9.36	No
41	11:52:51.95	44:05:47	63.0	8.12	12.83	1.04	3.12	6.47	7.96	Yes?
43	11:52:51.14	44:04:42	21.2	4.80	4.31	1.08	3.25	8.26	10.16	Yes?
46	11:52:50.58	44:06:28	16.7	4.24	3.39	1.08	3.23	2.68	3.30	No
47	11:52:50.52	44:04:36	94.1	9.95	19.09	1.05	3.16	23.81	29.29	Yes
49	11:52:50.39	44:08:06	107.4	10.86	21.82	1.10	3.29	18.28	22.48	No
50	11:52:50.23	44:07:11	26.1	5.39	5.31	1.10	3.31	6.84	8.41	No
51	11:52:49.59	44:07:16	36.0	6.40	7.31	1.14	3.42	4.80	5.90	No
52	11:52:49.01	44:07:17	15.2	4.12	3.08	1.12	3.36	3.73	4.59	No
53	11:52:48.92	44:05:28	20.3	4.69	4.12	1.08	3.25	4.04	4.97	No
56	11:52:47.19	44:06:59	16.2	4.24	3.28	1.12	3.35	2.03	2.50	No
59	11:52:46.74	44:09:04	13.4	4.12	2.73	1.26	3.79	3.33	4.10	No
61	11:52:46.44	44:07:53	46.8	7.28	9.52	1.13	3.39	16.49	20.28	Yes
63	11:52:46.26	44:06:28	92.7	9.80	18.79	1.04	3.12	14.76	18.15	No
65	11:52:44.47	44:09:14	19.5	5.00	3.97	1.29	3.86	7.18	8.83	No

Notes: SrcN = Source Number based on master source list; ‘Corr’d Ep2-Fx’ is the epoch 2 flux corrected for the build-up on the ACIS optical blocking window from Epoch 1 to Epoch 2; ‘3sigUnc’ = 3 times flux uncertainty to determine whether source is significantly variable or not. ‘Vary?’: ‘No’ or ‘Yes’ based on the comparison of the Epoch 1 flux + 3sigUnc versus the corrected Epoch 2 flux. Values lying with 3σ of each other warrant a ‘No.’ Values $> 3\sigma$ convert to ‘Yes.’ Values near that boundary warrant ‘Yes?’.

Based on the integrated H- α and 24 micron luminosities of two samples of nearby galaxies, Kennicutt et al. (2009) derived the following relation for the SFR of a galaxy:

$$\text{SFR (M}_{\odot} \text{ yr}^{-1}) = 7.9 \times 10^{-42} [L(H_{\alpha})_{obs} + 0.020L(24)] (\text{erg s}^{-1}).$$

In this equation, $L(H_{\alpha})_{obs}$ is the integrated H- α luminosity of the galaxy and $L(24)$ is equal to $\lambda * L_{24}$, where λ is the wavelength of the observation and L_{24} is the integrated spectral luminosity of the galaxy (in units of $\text{ergs s}^{-1} \text{ Hz}^{-1}$) at 24 microns. We determined $L(H_{\alpha})_{obs}$ for NGC 3938 as follows: based on the integrated H- α flux of $4.79 \times 10^{-12} \text{ ergs cm}^{-2} \text{ s}^{-1}$ from the galaxy as measured by Kennicutt & Kent (1983), we computed a corresponding integrated H- α luminosity of $2.77 \times 10^{41} \text{ ergs/s}$ using on our assumed distance to NGC 3938 of 22 Mpc. To compute $L(24)$, we adopted the integrated flux density at 24 microns of 1.09 Jy as measured by Dale et al. (2007) using the Multiband Imaging Photometer for Spitzer (MIPS) (Rieke et al. 2004) aboard the *Spitzer Space Telescope* (SST) (Werner et al. 2004). From this measured integrated flux density we computed an integrated spectral luminosity for NGC 3938 at 24 microns of $6.31 \times 10^{29} \text{ ergs s}^{-1} \text{ Hz}^{-1}$ and a value of $7.89 \times 10^{42} \text{ ergs s}^{-1}$ for $L(24)$. Combining the relation derived by Kennicutt et al. (2009) and our computed values for $L(H_{\alpha})_{obs}$ and $L(24)$, we obtain a value of 3.43 solar masses per year for the SFR of NGC 3938. For comparison, Caldú-Primo et al. (2009) compute an average SFR of 0.33 ± 0.09 solar masses per year using data from five different wavelength bands ranging from the ultraviolet through millimeter. We cannot easily account for the discrepancy between our computed SFR and the computed SFR presented by Caldú-Primo et al. (2009). Noting the large uncertainty in the distance to NGC 3938 (see §8), if we instead adopt a distance of 11 Mpc to NGC 3938, we compute an SFR of 0.86 solar masses per year. This value is a factor of ≈ 3 greater than the value determined by Caldú-Primo et al. (2009). We argue that an elevated SFR for NGC 3938 makes sense in light of the high historical supernova rate observed in this galaxy.

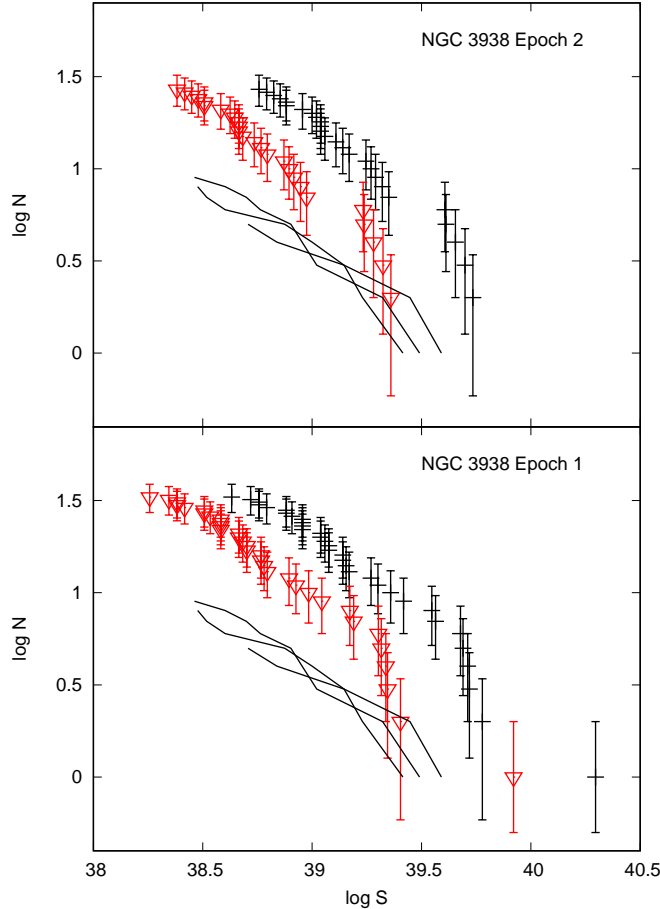
To determine the metallicity of NGC 3938 (as expressed in terms of $\log[\text{O}/\text{H}]$), we use the following relation for metallicity as derived by Lee et al. (2006):

$$12 \log [\text{O}/\text{H}] = 5.78 \pm 0.21 + (-0.122 \pm 0.012) M_{4.5}.$$

In this relation, $M_{4.5}$ is the absolute magnitude of NGC 3938 at the wavelength of 4.5 microns. We determined $M_{4.5}$ from the integrated flux density of 0.21 Jy measured at this wavelength by Dale et al. (2007) using the Infrared Array

Camera (IRAC) (Fazio et al. 2004) aboard the SST. From this measured flux density and adopting the standard IRAC 4.5 micron zero-magnitude flux density¹²

Figure 10. Luminosity function of the two observed epochs of NGC 3938, (data points with uncertainties) together with the ‘HMXB end’ of the luminosity functions of NGC 628, NGC 4321, and NGC 5194 (black lines). The NGC 3938 points are presented twice: using a distance of 20 Mpc (black points) and a distance of 13 Mpc (red points).



8. LUMINOSITY FUNCTION

Luminosity functions of X-ray binaries (XRBs) have received a considerable amount of attention since the launch of *Chandra*: e.g., Grimm et al. (2003), Gilfanov (2004), Binder et al. (2017), and perhaps culminating with Lehmer et al. (2019). Lehmer et al. (2019) analyzes the luminosity relations for 38 galaxies, including NGC 3938. We do not attempt to re-create any of these analyses nor even fit the luminosity function, dependent as it is upon the adopted distance.

Our first task is the expected number of background sources within the field-of-view. We can look at this in two ways: first, NGC 3938 essentially falls onto a single ACIS-I CCD, so the field-of-view is 64 sq arcmin. Adopting the background estimator from Campana et al. (2001), namely,

$$N(> L) = 360 \left(\frac{S}{2 \times 10^{-15}} \right)^{-0.68}$$

¹² See https://irsa.ipac.caltech.edu/data/SPITZER/docs/irac/iracinstrumenthandbook/IRAC_Instrument_Handbook.pdf. of 179.7, we computed an integrated apparent magnitude of 7.33 at this wavelength for NGC 3938. From this integrated apparent magnitude and our assumed distance of 22 Mpc to NGC 3938, we computed a value of -24.38 for $M_{4.5}$. Using this value for $M_{4.5}$ and the relation derived by Lee et al. (2006), we compute a range of values from 8.17 to 9.18 for $12 + \log [\text{O}/\text{H}]$. To put this result in context, we compared this computed metallicity with the metallicities of other galaxies of the same Hubble type as presented by Zaritsky et al. (1994). Those authors found a range of metallicities from 8.4 to 9.2 for Sc galaxies, therefore we conclude that our computed range of metallicity values are consistent with those of other Sc galaxies. In addition, Calzetti et al. (2007) analyzed SST IRAC and MIPS observations of NGC 3938 (at the wavelengths of $8 \mu\text{m}$ and $24 \mu\text{m}$) and estimated the metallicity $12 + \log [\text{O}/\text{H}]$ of the galaxy to range from 8.35 to 9.07, which is consistent with our computed range of values.

sources per square degree for a measured flux of S in $\text{erg s}^{-1} \text{cm}^{-2}$ in the 0.5-8 keV band then leads to five background sources. We have here assumed our minimum detectable threshold to be $\sim 3 \times 10^{-15} \text{ erg s}^{-1} \text{cm}^{-2}$. If we drop the minimum threshold to 2×10^{-15} , the number of sources rises to six. Alternatively, given that NGC 3938 occupies a smaller fraction of the CCD, we can also adopt the D25 circle. Using that for our area, then 2-3 sources on the NGC 3938 list (Table 3) are expected to be background objects.

Our second task is the adopted distance to NGC 3938. The NED¹³ lists essentially two different distances: ≈ 5 Mpc and ≈ 17 -22 Mpc. Figure 10 shows the XRB luminosity function assuming 13 and 20 Mpc distances. If we assume NGC 3938 matches the Milky Way in size, then its distance is closer to 16 Mpc. If we adopt its redshift and divide by an adopted H_0 of $70 \text{ km s}^{-1} \text{Mpc}^{-1}$, its distance should be ~ 11 Mpc. There is clearly a need to sort out the distance to NGC 3938. A distance of 10-12 Mpc would appear to match our NGC 3938 luminosity functions of Lehmer et al.

If we consider variability, the luminosity function does not differ significantly between the two epochs throughout the HMXB range from $\sim 10^{38}$ to $\sim 10^{39} \text{ erg s}^{-1}$. The distributions do differ at the high end where a single object is on in Epoch 1 and off in Epoch 2 (source 60). That result for NGC 3938 is in contrast to the results of Binder et al. (2017) for NGC 300, which proposed that a majority of outbursting X-ray binaries occur at sub-Eddington limits. While two epochs is a minimal sample, the difference may suggest a more active phase for NGC 300 and a less active phase for NGC 3938.

9. SUMMARY

Much of the discussion of our results occurred throughout the paper as we presented the data. A brief summary of our results follows.

We analyzed two epochs of *Chandra* observations of the face-on spiral NGC 3938. We detect a total of 95 sources within the galaxy from merging the data, with 66 and 48 sources detected for epochs 1 and 2, respectively. We attempt to use color hardness to classify the detected sources within the D25 circle. The contaminant on the ACIS Optical Blocking Window hampers that effort as it ‘collapses’ the color-color regional separation of the sources. Time variations are detected between the two epochs, correcting for the increased absorption of the ACIS optical blocking window, for about 1/4 of the sources in common between the two epochs. Only one source was detected to vary during an observation, but its location in a chip gap renders its detected variation unlikely. Only one source inside the D25 circle was particularly luminous – so a possible variable ULX candidate. NGC 3938 is sufficiently distant that we could not probe below $\approx 10^{38} \text{ erg s}^{-1}$ in the luminosity function. We also note a problem with the distance to NGC 3938 – on the basis of the multiple-galaxy-defined luminosity functions (Lehmer et al. 2019), the distance to NGC 3938 should fall in the 10-12 Mpc band, not the ~ 5 Mpc nor 17-22 Mpc bands that dominate the NED values.

We also briefly describe the sources detected by *Chandra* that lie *outside* of the D25 circle of NGC 3938. Approximately sixty percent of those sources have known counterparts. Of the remaining forty percent, half have one or two apparent counterparts within the detection region, requiring relatively straightforward confirmation of the X-ray source’s counterpart.

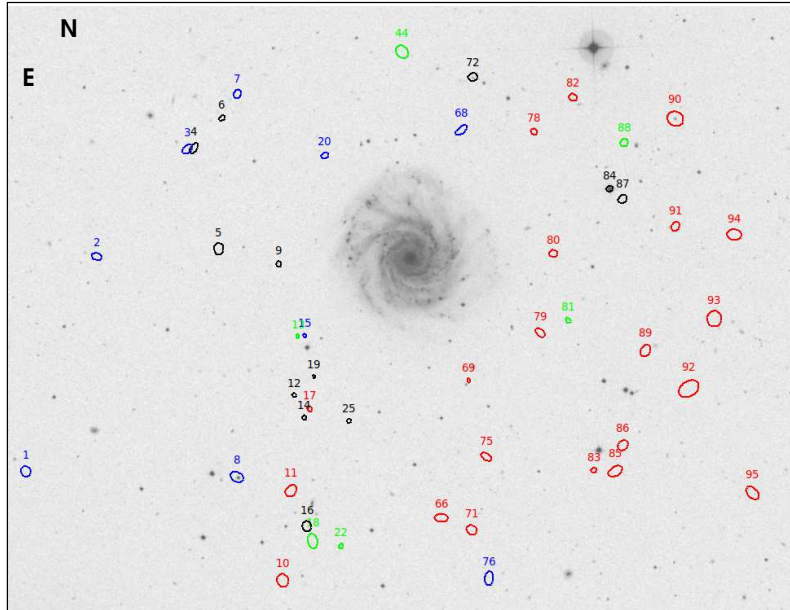
We thank the anonymous referee for comments that improved this paper. This research has made use of the NASA/IPAC Infrared Science Archive (IRSA) and the NASA/IPAC Extragalactic Database, both of which are funded by the National Aeronautics and Space Administration and operated by the California Institute of Technology. This research has also made use of NASA’s Astrophysics Data System. The ADS is operated by the Smithsonian Astrophysical Observatory under NASA Cooperative Agreement 80NSSC21M0056. We also used images obtained by the NASA/ESA Hubble Space Telescope obtained from the Space Telescope Science Institute, which is operated by the Association of Universities for Research in Astronomy, Inc., under NASA contract NAS 5-26555. These observations are associated with program 16239. This research has made use of data obtained from the Chandra Data Archive at the Chandra X-ray Center. This paper employs a list of Chandra data sets, obtained by the Chandra X-ray Observatory, contained in [DOI:10.25575/cdc.258](https://doi.org/10.25575/cdc.258).

¹³ NASA Extragalactic Database, ned.ipac.caltech.edu

Facilities: CXO, ADS, IRSA, Spitzer, WISE, NED, MAST, HST

Software: CIAO (Fruscione et al. 2006)

Figure 11. The *Chandra*-detected sources outside of the D25 circle of NGC 3938. The image is $\sim 20'$ on a side.



APPENDIX

A. SOURCES DETECTED OUTSIDE D25

A.1. CSC correspondence

Figure 11 shows the 47 detected sources outside of the D25 circle. Of that 47, seven are not listed as a CSC source (our merged numbers 1, 3, 4, 10, 15, 18, and 44). Of those, 1 and 10 lie on the edge of a CCD and could easily have been dropped by imposing a minimum distance to the CCD edge. We elected not to impose such a minimum. Two additional sources (18, 44) are only detected in the merged data. The CSC catalog does not contain merged-epoch detections if the pointings between multiple observations are greater than $1'$. There remain three sources (3, 4, 15) for which we have no explanation why they were not included on the CSC list.

Table 6. Sources in CSC, Outside D25 and Below Our Detection Threshold

CSC ID	CSC ID	CSC ID
<i>2CXO J115220.8+440605</i>	<i>2CXO J115218.7+440505</i>	<i>2CXO J115227.7+440230</i>
<i>2CXO J115207.7+440431</i>	<i>2CXO J115205.6+440845</i>	<i>2CXO J115203.6+440354</i>
<i>2CXO J115250.8+435811</i>	<i>2CXO J115218.3+441424</i>	<i>2CXO J115153.1+440709</i>
<i>2CXO J115153.6+440503</i>	<i>2CXO J115217.2+435816</i>	<i>2CXO J115212.0+435843</i>
<i>2CXO J115201.4+440012</i>	<i>2CXO J115348.0+440242</i>	<i>2CXO J115351.7+440417</i>
<i>2CXO J115203.3+435825</i>		

Sources in *italics* are listed as ‘marginal’ in the CSC catalog.

Tackling the same question from the other direction finds 24 sources on the CSC list that were not detected by us. Five of those sources are automatically excluded by us – the CSC team elected to process *all* of the CCDs whereas we opted to process only those near the aimpoint. For ACIS-I, that means we include CCDs I0 to I3, but not S3 and S4 which are typically active during an “ACIS-I” observation. For the analysis in this paper, those five sources lie outside

the I0 to I3 CCDs. An additional sixteen CSC sources lie below our detection threshold. Those sources are listed in Table A.1. Of the sixteen, the CSC lists eleven as ‘marginal.’

That leaves just three sources: 2CXO J115246.1+440147; 2CXO J115223.3+440342; and 2CXO J115209.7+441405. The last one is listed as ‘marginal’ in the CSC catalog. The first two appear to lie above our detection threshold. However, we do not detect them, yet they appear to match the *Chandra* PSF at their off-axis angles. We have looked closely at the detection parameters and can not provide a ready explanation for the two non-detections.

A.2. Identification of Sources Outside D25

Returning to our detected sources that lie outside D25, if we adopt the source classifications available from NED without question, we then have the results shown in Table A.2 and listed in the ‘Cntrprt’ column of Table 3 (outside). We do not use the color-color approach as it was built for separation of X-ray binaries and not galaxies and AGN.

The ‘IR source’ category would benefit from additional investigation – some sources are clearly separated into ‘star’ or ‘galaxy’ while the IR sources are unknown at the present time. Further, the ‘unknown’ category could also be investigated: one can overlay the *Chandra* region files for the undetected sources onto an IRAC image (eg, 3.6μ) and find matches, or at least candidates, for *all* of the ‘unknown’ X-ray sources (q.v., ‘Cntrprt’ column in Table 3 (outside)). However, tracking down or characterizing these identifications lies outside the scope of this paper.

Table 7. Source Identification: *Outside D25* (NED)

Type	Number	Source Numbers
star	5	2, 5, 16, 84, 93
galaxy	13	4, 7, 9, 13, 17, 18, 19, 22, 25, 66, 71, 72, 91
IR source	7	6, 20, 44, 69, 75, 78, 79, 86
QSO	1	14
Radio source	1	87
No classification	20	1, 3, 8, 10, 11, 12, 15, 68, 76, 78, 80 81, 82, 83, 85, 88, 89, 90, 92, 94, 95

%endfigure

A.3. Timing Variations for Sources Outside D25

We also examine the variation between Epochs 1 and 2 for sources outside the D25 circle (Table 8). We take the same approach as we did for those sources inside D25 – sources within an epoch via CIAO.g1vary (next paragraphs) and sources across epochs via the Epoch 1 vs Epoch 2 counts.

For the sources outside D25, there are two other categories to be assessed. The first category consists of sources observed in Epoch 1 *or* Epoch 2 that were observed one time and did not fall within the detector’s field-of-view during the other epoch. For Epoch 1, those sources are 10, 83, 85, 86, and 89 to 95; for epoch 2, the sources are 1 to 5, 8, and 44. Of these two sets, only source 94 was detected by the g1vary routine as variable within an observation with an index of 6 indicating near-certainty of variation. Given that it was detected with ~ 22 counts and given that it does not lie on a chip edge, it is quite possible that its variation is real.

The second category consists of those source that *could* have been detected twice because both fields-of-view covered the source’s position, but each source was only detected once. Within this category there are two sub-categories: (i) there was one detection of a somewhat weak source that was not detected a second time because of the reduced sensitivity owing to a greater off-axis observation or the increased contaminant on the optical blocking window; and (ii) the source was actually off during one of the observations.

For Epoch 1, the sources that were on but were not detected during Epoch 2 are 11, 17, 66, 69, 71, 75, 78, 79, 80, and 82. The corresponding sources for Epoch 2 are sources 7, 13, 20, 68, and 76. We first eliminate the ‘near chip gap’ or ‘larger off-axis angle’ objects (Ep 1: 11, 17, 79, 82; Ep 2: 7, 68).

Clearly, the second sub-category is more interesting than the first. For Epoch 1, the sources for which the position falls well within the detector for *both* epochs are 66, 69, 71, 75, 78, and 80; the corresponding sources for Epoch 2 are 20 and 76. All of these sources are relatively weak with total counts in the ~ 17 to ~ 32 range. However, while weak, they all have sufficient counts that even with the ACIS window increase between the epochs, detections would have

Table 8. Epoch 1 versus Epoch 2 for Sources Outside the D25 circle

SrcN	RA (J2000)	Dec (J2000)	Ep-1 Cts	Ep-1 Unc	Ep-1 Flux	Flux Unc	3sig Unc	Ep-2 Flux	Corr'd Ep2-Fx	Vary? ^a
4	11:53:26.52	44:10:35	10.1	4.00	2.05	1.58	4.75	4.03	4.96	No
5	11:53:22.09	44:07:30	55.8	8.66	11.31	1.34	4.03	5.68	6.99	Yes?
6	11:53:21.57	44:11:31	43.9	8.60	8.93	1.69	5.06	8.78	10.80	No
9	11:53:11.74	44:07:03	25.9	6.25	5.27	1.51	4.52	3.15	3.87	Yes?
12	11:53:09.05	44:03:01	16.1	5.39	3.26	1.80	5.40	5.34	6.57	Yes?
14	11:53:07.46	44:02:19	84.3	9.95	17.17	1.17	3.52	10.55	12.98	Yes?
16	11:53:07.05	43:58:59	27.3	6.00	5.54	1.32	3.96	6.97	8.57	No
19	11:53:05.81	44:03:35	81.3	9.27	16.56	1.06	3.17	9.47	11.65	Yes?
25	11:52:59.72	44:02:13	12.0	4.00	2.40	1.34	4.01	7.75	9.53	Yes?
72	11:52:38.72	44:12:47	297.7	18.47	60.50	1.15	3.44	89.03	109.51	Yes
84	11:52:15.28	44:09:21	26.7	6.86	5.32	1.76	5.29	5.13	6.31	No
87	11:52:13.11	44:09:03	110.4	12.73	22.42	1.46	4.39	13.76	16.92	Yes?

Notes: SrcN = SouRCe Number based on master source list; ‘Corr’d Ep2-Fx’ is the EPOCH 2 FluX CORRECTed for the build-up on the ACIS optical blocking window from Epoch 1 to Epoch 2; ‘3sigUnc’ = 3 times the flux UNCertainty to determine whether the source is significantly variable.

^aVary: to determine variability, the Epoch 1 flux and its uncertainty are compared to the corrected Epoch 2 flux. Values lying within 3σ of each other warrant a ‘No’. Values $> 3\sigma$ convert to ‘Yes’. Values near the boundary warrant ‘Yes?’.

been possible *if* each source had remained constant. Consequently, we deem all of the Epoch 1 sources as ‘on’ during Epoch 1 and ‘off’ during Epoch 2. The opposite situation applies to sources 20 and 68: ‘off’ during Epoch 1 but ‘on’ during Epoch 2.

Source 76 was detected during Epoch 2, but not during Epoch 1. The source, however, happens to lie near the edge of *both* observations. We consequently deem it ‘off’ during Epoch 1 and ‘on’ during Epoch 2, but it is possible that it suffers from lying too close to a chip edge.

Finally, there are variations possible within an observation for the sources outside D25 and not discussed above in the single-epoch paragraph. Most sources exhibit no variations. **G1vary** reports three variables: sources 14, 19, and 88. Of these, source 88 can be eliminated quickly as it has ~ 35 counts, is detected only in the merged data, and lies near a chip edge for Epoch 2. Sources 14 and 19 both lie near a chip gap, but have sufficiently large Epoch 1 counts that the drop to Epoch 2 suggests variability. The ‘within-Epoch’ variability is likely caused by their locations near the chip gap.

B. INDIVIDUAL EPOCH TABLES

B.1. *Detected Source Tables*

The detected source tables are placed in this appendix solely to make the article pages easier to read. As stated in the analysis section, ‘N’ refers to the *merged* source number and is used for both epochs of data.

B.2. *Color-color tables*

The color-color tables are placed in this appendix solely to make the article pages easier to read. We divide both tables into ‘within the D25 circle’ and ‘outside D25’. As stated in the analysis section, ‘N’ refers to the source number in the *merged* source list and is used for both epochs of data.

Table 9. NGC 3938: Epoch 1 Detected Sources^a

N	RA	Dec	Counts	Err	BkgCts	BkEr	SrcRate	SrcRErr	BkgRate	BkRErr	Signif	Flux ^b	L _X ^c
Inside D25 circle													
21	11:53:03.84	44:08:46.21	33.7	6.93	14.3	0.09	6.79e-04	1.39e-04	2.87e-04	1.90e-06	6.9	6.86	3.9
23	11:53:00.25	44:05:59.87	85.4	9.54	5.6	0.05	1.72e-03	1.92e-04	1.12e-04	1.06e-06	24.3	17.37	10.0
24	11:53:00.14	44:07:00.33	25.7	5.48	4.3	0.05	5.17e-04	1.10e-04	8.72e-05	9.40e-07	7.9	5.22	3.0
27	11:52:57.15	44:08:08.41	65.7	8.43	5.3	0.05	1.32e-03	1.70e-04	1.07e-04	1.03e-06	19.0	13.33	7.7
28	11:52:56.09	44:04:12.09	9.7	3.32	1.3	0.02	1.96e-04	6.67e-05	2.56e-05	5.02e-07	4.0	1.98	1.1
31	11:52:54.73	44:09:16.49	10.1	3.74	3.9	0.04	2.04e-04	7.53e-05	7.81e-05	8.88e-07	3.2	2.06	1.2
32	11:52:54.72	44:07:51.88	87.7	9.64	5.3	0.05	1.77e-03	1.94e-04	1.06e-04	1.04e-06	25.4	17.88	10.3
33	11:52:54.70	44:05:28.77	25.0	5.20	2.0	0.03	5.04e-04	1.05e-04	3.95e-05	6.22e-07	9.5	5.09	2.9
37	11:52:53.77	44:07:34.43	20.0	4.80	3.0	0.04	4.03e-04	9.65e-05	6.00e-05	7.59e-07	6.8	4.07	2.3
38	11:52:53.51	44:06:12.29	41.0	6.56	2.0	0.03	8.24e-04	1.32e-04	4.09e-05	6.28e-07	15.4	8.32	4.8
39	11:52:53.04	44:07:11.33	25.0	5.20	2.0	0.03	5.03e-04	1.05e-04	3.99e-05	6.29e-07	9.4	5.08	2.9
41	11:52:51.95	44:05:47.44	63.0	8.12	3.0	0.04	1.27e-03	1.63e-04	5.97e-05	7.81e-07	21.5	12.83	7.4
42	11:52:51.60	44:03:43.92	16.3	4.24	1.7	0.03	3.28e-04	8.54e-05	3.37e-05	5.68e-07	6.4	3.31	1.9
43	11:52:51.14	44:04:41.94	21.2	4.80	1.8	0.03	4.27e-04	9.65e-05	3.53e-05	5.87e-07	8.2	4.31	2.5
45	11:52:50.80	44:06:53.31	8.1	3.16	1.9	0.03	1.63e-04	6.36e-05	3.87e-05	6.11e-07	3.1	1.65	0.9
46	11:52:50.58	44:06:27.82	16.7	4.24	1.3	0.02	3.36e-04	8.54e-05	2.63e-05	4.99e-07	6.9	3.39	1.9
47	11:52:50.52	44:04:35.66	94.1	9.95	4.9	0.05	1.89e-03	2.00e-04	9.86e-05	1.01e-06	27.9	19.09	11.0
49	11:52:50.39	44:08:06.18	107.4	10.86	10.6	0.07	2.16e-03	2.19e-04	2.13e-04	1.48e-06	24.6	21.82	12.6
50	11:52:50.23	44:07:11.25	26.1	5.39	2.9	0.04	5.26e-04	1.08e-04	5.79e-05	7.70e-07	9.0	5.31	3.1
51	11:52:49.59	44:07:16.27	36.0	6.40	5.0	0.05	7.24e-04	1.29e-04	1.01e-04	9.98e-07	10.6	7.31	4.2
52	11:52:49.01	44:07:17.40	15.2	4.12	1.8	0.03	3.05e-04	8.30e-05	3.68e-05	5.91e-07	5.8	3.08	1.7
53	11:52:48.92	44:05:28.44	20.3	4.69	1.7	0.03	4.08e-04	9.44e-05	3.47e-05	5.81e-07	7.9	4.12	2.4
56	11:52:47.19	44:06:58.65	16.2	4.24	1.8	0.03	3.25e-04	8.54e-05	3.69e-05	5.93e-07	6.2	3.28	1.9
58	11:52:46.86	44:10:07.77	16.2	5.00	8.8	0.07	3.26e-04	1.01e-04	1.78e-04	1.51e-06	4.0	3.29	1.9
59	11:52:46.74	44:09:03.59	13.4	4.12	3.6	0.04	2.70e-04	8.30e-05	7.23e-05	8.45e-07	4.3	2.73	1.6
60	11:52:46.65	44:06:48.45	354.5	19.13	11.5	0.08	7.13e-03	3.85e-04	2.31e-04	1.54e-06	78.9	71.91	41.5
61	11:52:46.44	44:07:53.24	46.8	7.28	6.2	0.06	9.43e-04	1.46e-04	1.24e-04	1.11e-06	12.9	9.52	5.5
62	11:52:46.33	44:03:52.53	10.0	3.32	1.0	0.02	2.02e-04	6.67e-05	1.98e-05	4.34e-07	4.3	2.04	1.2
63	11:52:46.26	44:06:27.71	92.7	9.80	3.3	0.04	1.86e-03	1.97e-04	6.71e-05	8.30e-07	30.7	18.79	10.8
64	11:52:45.64	44:05:26.68	13.8	3.87	1.2	0.02	2.79e-04	7.79e-05	2.32e-05	4.76e-07	5.8	2.82	1.6
65	11:52:44.47	44:09:14.20	19.5	5.00	5.5	0.05	3.93e-04	1.01e-04	1.10e-04	1.05e-06	5.6	3.97	2.3
70	11:52:38.95	44:06:02.49	21.5	4.80	1.5	0.03	4.32e-04	9.65e-05	3.07e-05	5.48e-07	8.6	4.36	2.5
77	11:52:34.44	44:05:16.27	10.7	3.46	1.3	0.03	2.16e-04	6.97e-05	2.59e-05	5.10e-07	4.4	2.19	1.3
Outside D25 circle													
4	11:53:26.52	44:10:34.65	10.1	4.00	5.9	0.06	2.03e-04	8.05e-05	1.19e-04	1.22e-06	2.8	2.05	1.2
5	11:53:22.09	44:07:29.95	55.8	8.66	19.2	0.11	1.12e-03	1.74e-04	3.87e-04	2.23e-06	10.2	11.31	6.5
6	11:53:21.57	44:11:31.38	43.9	8.60	30.1	0.14	8.84e-04	1.73e-04	6.05e-04	2.79e-06	6.7	8.93	5.1
9	11:53:11.74	44:07:03.09	25.9	6.25	13.1	0.09	5.22e-04	1.26e-04	2.63e-04	1.80e-06	5.5	5.27	3.0
10	11:53:11.11	43:57:19.53	73.6	9.85	23.4	0.12	1.48e-03	1.98e-04	4.70e-04	2.46e-06	12.5	14.95	8.6
11	11:53:09.67	44:00:04.79	29.2	6.86	17.8	0.11	5.88e-04	1.38e-04	3.57e-04	2.15e-06	5.5	5.94	3.4
12	11:53:09.05	44:03:00.92	16.1	5.39	12.9	0.09	3.23e-04	1.08e-04	2.60e-04	1.79e-06	3.4	3.26	1.9
14	11:53:07.46	44:02:19.47	84.3	9.95	14.7	0.09	1.70e-03	2.00e-04	2.97e-04	1.91e-06	17.1	17.17	9.9
16	11:53:07.05	43:58:58.78	27.3	6.00	8.7	0.07	5.49e-04	1.21e-04	1.75e-04	1.45e-06	6.7	5.54	3.1
17	11:53:06.57	44:02:36.21	39.8	7.68	19.2	0.11	8.00e-04	1.55e-04	3.87e-04	2.21e-06	7.3	8.08	4.7
19	11:53:05.81	44:03:34.88	81.3	9.27	4.7	0.05	1.64e-03	1.87e-04	9.55e-05	9.81e-07	24.3	16.56	9.5
25	11:52:59.72	44:02:12.99	12.0	4.00	4.0	0.04	2.41e-04	8.05e-05	8.13e-05	8.95e-07	3.7	2.43	1.4
66	11:52:44.20	43:59:14.67	25.0	6.56	18.0	0.11	5.03e-04	1.32e-04	3.62e-04	2.13e-06	4.7	5.08	2.9
69	11:52:39.35	44:03:27.68	23.2	5.00	1.8	0.03	4.66e-04	1.01e-04	3.68e-05	6.01e-07	8.9	4.70	2.7
71	11:52:38.93	43:58:52.25	24.1	6.33	15.9	0.10	4.85e-04	1.27e-04	3.20e-04	2.02e-06	4.7	4.90	2.8
72	11:52:38.72	44:12:46.71	297.7	18.47	43.3	0.17	5.99e-03	3.72e-04	8.72e-04	3.40e-06	39.0	60.50	34.9
75	11:52:36.43	44:01:07.42	17.6	5.39	11.4	0.08	3.53e-04	1.08e-04	2.30e-04	1.68e-06	3.9	3.56	2.0
78	11:52:28.24	44:11:06.32	17.4	5.57	13.6	0.09	3.50e-04	1.12e-04	2.74e-04	1.85e-06	3.6	3.53	2.0
79	11:52:27.12	44:04:54.49	18.1	4.69	3.9	0.04	3.64e-04	9.44e-05	7.88e-05	8.97e-07	5.7	3.68	2.1
80	11:52:25.04	44:07:22.40	22.2	6.25	16.8	0.10	4.46e-04	1.26e-04	3.39e-04	2.05e-06	4.3	4.51	2.6
82	11:52:21.44	44:12:08.93	35.2	7.28	17.8	0.11	7.08e-04	1.47e-04	3.59e-04	2.13e-06	6.6	7.15	4.1
83	11:52:18.05	44:00:42.87	26.1	6.71	18.9	0.11	5.24e-04	1.35e-04	3.81e-04	2.19e-06	4.8	5.29	3.0
84	11:52:15.28	44:09:20.71	26.7	6.86	20.3	0.11	5.37e-04	1.38e-04	4.08e-04	2.27e-06	4.8	5.42	3.1
85	11:52:14.41	44:00:40.70	47.2	8.37	22.8	0.12	9.51e-04	1.68e-04	4.58e-04	2.41e-06	8.1	9.60	5.5
86	11:52:13.10	44:01:28.22	63.7	9.33	23.3	0.12	1.28e-03	1.88e-04	4.70e-04	2.43e-06	10.8	12.93	7.5
87	11:52:13.11	44:09:02.54	110.4	12.73	51.6	0.18	2.22e-03	2.56e-04	1.04e-03	3.66e-06	13.4	22.42	12.9
89	11:52:09.24	44:04:22.25	28.5	6.78	17.5	0.10	5.73e-04	1.36e-04	3.52e-04	2.11e-06	5.4	5.78	3.3
90	11:52:04.12	44:08:10.54	26.1	7.14	24.9	0.13	5.25e-04	1.44e-04	5.01e-04	2.53e-06	4.3	5.30	3.0
91	11:52:04.06	44:11:29.88	44.4	9.38	43.6	0.17	8.94e-04	1.89e-04	8.77e-04	3.35e-06	5.8	9.03	5.2
92	11:52:01.68	44:03:13.27	84.5	12.45	70.5	0.21	1.70e-03	2.51e-04	1.42e-03	4.27e-06	9.0	17.17	9.9
93	11:51:57.46	44:05:21.48	39.1	8.72	36.9	0.15	7.87e-04	1.75e-04	7.42e-04	3.08e-06	5.5	7.95	4.6
94	11:51:54.01	44:07:55.66	22.3	6.93	25.7	0.13	4.49e-04	1.39e-04	5.17e-04	2.57e-06	3.6	4.53	2.6
95	11:51:50.98	43:59:59.96	33.5	7.88	28.5	0.14	6.74e-04	1.58e-04	5.73e-04	2.74e-06	5.2	6.81	3.9

^aColumn headings are defined as: ‘N’ = source number from the *merged* source list; ‘RA’, ‘Dec’ = source position, J2000, and sorted by decreasing RA; ‘Counts’, ‘Err’ = *wavdetect*-determined source counts and uncertainty; ‘BkgCts’, ‘BkgErr’ = *wavdetect*-determined background counts and uncertainty; ‘SrcRate’, ‘SrcRErr’ = source count rate and uncertainty rate = SrcCts / exposureTime; ‘BkgRate’, ‘BkgRErr’ = background count rate and uncertainty rate and determined in the same manner as the ‘SrcRate’ and ‘SrcRErr’; ‘Signif’ = statistical significance as determined by *wavdetect*; ‘SrcFlux’ and ‘L_X’ = Source Flux and Luminosity. The count rates were converted to fluxes using WebPIMMS with an adopted absorbed thermal bremsstrahlung model of 5 keV. We do not include uncertainties because we do not know the source model.

^bAbsorbed flux in the 0.5 - 8 keV band in units of 10^{-15} erg s⁻¹ cm⁻².
^cAbsorbed luminosity in the 0.5 - 8 keV band in units of 10^{38} erg s⁻¹ assuming a distance of 22 Mpc. If the distance is 17 Mpc, the luminosities will decrease by a factor of 0.59.

Table 10. NGC 3938 Epoch 2 Detected Source List^a

N	RA	Dec	Counts	Err	BkgCts	BkEr	SrcRate	SrcRErr	BkgRate	BkRErr	Signif	Flux ^b	L _X ^c
Inside D25 circle													
21	11:53:03.92	44:08:46.46	15.6	4.12	1.4	0.03	3.43e-04	9.06e-05	3.04e-05	5.76e-07	6.3	4.25	2.4
23	11:53:00.25	44:06:00.43	54.5	7.48	1.5	0.03	1.20e-03	1.64e-04	3.34e-05	6.08e-07	21.7	14.88	8.6
26	11:52:57.58	44:06:47.34	10.6	3.46	1.4	0.03	2.33e-04	7.61e-05	3.04e-05	5.54e-07	4.3	2.89	1.6
29	11:52:55.24	44:09:05.08	14.1	4.24	3.9	0.04	3.10e-04	9.32e-05	8.60e-05	9.83e-07	4.5	3.84	2.2
30	11:52:54.84	44:07:36.10	8.6	3.16	1.4	0.03	1.89e-04	6.95e-05	3.02e-05	5.57e-07	3.5	2.34	1.3
31	11:52:54.76	44:09:17.18	10.0	3.61	3.0	0.04	2.20e-04	7.92e-05	6.54e-05	8.40e-07	3.4	2.73	1.6
32	11:52:54.70	44:07:52.34	72.9	8.78	4.1	0.05	1.60e-03	1.93e-04	8.91e-05	9.94e-07	22.9	19.84	11.4
33	11:52:54.68	44:05:29.09	15.0	4.00	1.0	0.02	3.29e-04	8.79e-05	2.27e-05	4.90e-07	6.4	4.08	2.3
34	11:52:54.46	44:06:58.67	14.8	4.00	1.2	0.02	3.26e-04	8.79e-05	2.59e-05	5.19e-07	6.2	4.04	2.3
37	11:52:53.71	44:07:34.74	18.9	4.58	2.1	0.03	4.15e-04	1.01e-04	4.65e-05	7.07e-07	7.0	5.15	2.9
38	11:52:53.49	44:06:12.83	27.9	5.48	2.1	0.03	6.14e-04	1.20e-04	4.53e-05	6.99e-07	10.4	7.61	4.4
41	11:52:51.92	44:05:47.92	23.8	5.00	1.2	0.02	5.22e-04	1.10e-04	2.69e-05	5.39e-07	9.9	6.47	3.7
43	11:52:51.13	44:04:42.57	30.3	6.08	6.7	0.06	6.66e-04	1.34e-04	1.47e-04	1.27e-06	8.1	8.26	4.7
46	11:52:50.57	44:06:28.33	9.8	3.32	1.2	0.02	2.16e-04	7.29e-05	2.57e-05	5.14e-07	4.1	2.68	1.5
47	11:52:49.56	44:04:36.26	87.3	9.59	4.7	0.05	1.92e-03	2.11e-04	1.02e-04	1.07e-06	26.3	23.81	13.7
49	11:52:50.34	44:08:06.64	66.8	8.37	3.2	0.04	1.47e-03	1.84e-04	7.02e-05	8.81e-07	22.4	18.28	10.5
50	11:52:50.22	44:07:11.63	25.1	5.29	2.9	0.04	5.52e-04	1.16e-04	6.31e-05	8.33e-07	8.7	6.84	3.9
51	11:52:49.56	44:07:17.22	17.6	4.58	3.4	0.04	3.87e-04	1.01e-04	7.44e-05	8.96e-07	5.8	4.80	2.7
52	11:52:48.98	44:07:17.75	13.7	4.00	2.3	0.03	3.01e-04	8.79e-05	5.10e-05	7.49e-07	5.0	3.73	2.1
53	11:52:48.91	44:05:28.67	14.8	4.00	1.2	0.02	3.26e-04	8.79e-05	2.57e-05	5.18e-07	6.2	4.04	2.3
54	11:52:48.10	44:07:03.70	9.3	3.32	1.7	0.03	2.04e-04	7.29e-05	3.75e-05	6.23e-07	3.6	2.53	1.4
56	11:52:47.20	44:06:59.15	7.5	3.00	1.5	0.03	1.64e-04	6.59e-05	3.37e-05	6.05e-07	3.0	2.03	1.2
59	11:52:46.65	44:09:04.67	12.2	4.00	3.8	0.04	2.69e-04	8.79e-05	8.28e-05	9.49e-07	3.9	3.33	1.9
61	11:52:46.48	44:07:53.85	60.5	8.12	5.5	0.05	1.33e-03	1.78e-04	1.21e-04	1.16e-06	17.3	16.49	9.5
63	11:52:46.24	44:06:28.30	54.3	7.68	4.7	0.05	1.19e-03	1.69e-04	1.04e-04	1.04e-06	16.3	14.76	8.5
65	11:52:44.46	44:09:14.94	26.3	5.57	4.7	0.05	5.78e-04	1.22e-04	1.03e-04	1.05e-06	7.9	7.17	4.1
74	11:52:36.88	44:07:56.70	19.9	6.33	20.1	0.11	4.37e-04	1.39e-04	4.42e-04	2.51e-06	3.6	5.42	3.1
Outside D25 circle													
1	11:53:54.95	44:00:39.43	17.8	5.57	13.2	0.09	3.91e-04	1.22e-04	2.90e-04	2.03e-06	3.8	4.85	2.8
2	11:53:42.85	44:07:15.65	42.7	7.94	20.3	0.11	9.37e-04	1.74e-04	4.47e-04	2.50e-06	7.6	11.16	6.4
3	11:53:27.49	44:10:33.19	24.8	6.33	15.2	0.10	5.44e-04	1.39e-04	3.35e-04	2.16e-06	5.0	6.75	3.9
4	11:53:26.35	44:10:36.64	14.8	5.20	12.2	0.09	3.25e-04	1.14e-04	2.68e-04	1.93e-06	3.2	4.03	2.3
5	11:53:21.96	44:07:30.69	20.9	5.00	4.1	0.04	4.58e-04	1.10e-04	9.10e-05	9.88e-07	6.5	5.68	3.3
6	11:53:21.61	44:11:31.16	32.2	6.40	8.8	0.07	7.08e-04	1.41e-04	1.93e-04	1.61e-06	7.9	8.78	5.1
7	11:53:18.99	44:12:14.52	17.3	5.39	11.7	0.08	3.81e-04	1.18e-04	2.56e-04	1.87e-06	3.8	4.72	2.7
8	11:53:18.92	44:00:30.15	21.2	6.08	15.8	0.10	4.66e-04	1.34e-04	3.47e-04	2.19e-06	4.2	5.78	3.3
9	11:53:11.85	44:07:02.53	11.6	3.61	1.4	0.03	2.54e-04	7.92e-05	3.14e-05	5.70e-07	4.7	3.15	1.8
12	11:53:09.22	44:03:01.57	19.6	5.00	5.4	0.05	4.31e-04	1.10e-04	1.18e-04	1.13e-06	5.7	5.34	3.1
13	11:53:07.39	44:04:50.65	14.1	4.00	1.9	0.03	3.10e-04	8.79e-05	4.11e-05	6.58e-07	5.4	3.84	2.2
14	11:53:07.38	44:02:20.37	38.7	6.93	9.3	0.08	8.51e-04	1.52e-04	2.04e-04	1.65e-06	9.3	10.55	6.1
16	11:53:07.03	43:59:00.44	25.6	6.86	21.4	0.12	5.62e-04	1.51e-04	4.71e-04	2.56e-06	4.5	6.97	4.0
19	11:53:05.80	44:03:34.66	34.8	6.16	3.2	0.04	7.64e-04	1.35e-04	7.06e-05	8.91e-07	11.6	9.47	5.5
20	11:53:04.03	44:10:22.25	25.5	5.48	4.5	0.05	5.61e-04	1.20e-04	9.82e-05	1.02e-06	7.8	6.96	4.0
25	11:52:59.85	44:02:13.49	28.5	6.48	13.5	0.09	6.25e-04	1.42e-04	2.97e-04	2.02e-06	6.0	7.75	4.5
68	11:52:40.71	44:11:09.34	15.0	5.10	11.0	0.08	3.29e-04	1.12e-04	2.42e-04	1.80e-06	3.4	4.08	2.3
72	11:52:38.75	44:12:47.34	326.9	19.29	45.1	0.17	7.18e-03	4.24e-04	9.91e-04	3.75e-06	42.1	89.03	51.4
76	11:52:35.96	43:57:25.09	32.4	7.55	24.6	0.13	7.12e-04	1.66e-04	5.40e-04	2.75e-06	5.4	8.83	5.1
84	11:52:15.20	44:09:20.64	18.8	5.83	15.2	0.10	4.14e-04	1.28e-04	3.33e-04	2.14e-06	3.8	5.13	2.9
87	11:52:12.97	44:09:01.63	50.6	8.95	29.4	0.14	1.11e-03	1.97e-04	6.47e-04	3.04e-06	7.8	13.76	7.9

^aSee footnote 'a' to the Epoch 1 table. The columns are identically defined.^bAbsorbed flux in units of 10^{-15} erg s⁻¹ cm⁻² in the 0.5 - 8.0 keV band.^cAbsorbed luminosity in the 0.5 - 8 keV band in units of 10^{38} erg s⁻¹ assuming a distance of 22 Mpc. If the distance is 17 Mpc, the luminosities will decrease by a factor of 0.59.

Table 11. Color-Color Results By Source: Epoch 1^a

N	RA	Dec	BCts	BUnc	SCts	SUnc	MCts	MUnc	HCts	HUnc	M-S/B	UM-S/B	H-M/B	UH-S/B
Within D25 circle														
21	11:53:03.84	44:08:46.21	33.7	6.93	0.0	3.1	11.4	3.46	10.6	3.74	0.246	0.2623	-0.024	0.0121
23	11:53:00.25	44:05:59.87	85.4	9.54	6.8	2.65	36.7	6.08	42.4	6.63	0.350	0.1533	0.067	0.0169
24	11:53:00.14	44:07:00.33	25.7	5.48	0.0	3.1	13.5	3.74	10.9	3.46	0.405	0.4287	-0.101	0.0478
27	11:52:57.15	44:08:08.41	65.7	8.43	11.1	3.46	44.4	6.71	10.3	3.46	0.507	0.1872	-0.519	0.2025
28	11:52:56.09	44:04:12.09	9.7	3.32	0.0	3.1	0.0	4.90	0.0	3.20	0.186	0.2700	-0.175	0.2550
31	11:52:54.73	44:09:16.49	10.1	3.74	0.0	3.1	4.7	2.24	0.0	3.20	0.158	0.1850	-0.465	0.5435
32	11:52:54.72	44:07:51.88	87.7	9.64	11.5	3.46	44.4	6.78	32.6	5.83	0.375	0.1331	-0.135	0.0349
33	11:52:54.70	44:05:28.77	25.0	5.20	0.0	3.1	15.7	4.00	7.6	2.83	0.504	0.5306	-0.324	0.1610
37	11:52:53.77	44:07:34.43	20.0	4.80	0.0	3.1	8.6	3.00	11.9	3.61	0.275	0.2986	0.165	0.0859
38	11:52:53.51	44:06:12.29	41.0	6.56	0.0	3.1	15.7	4.00	22.2	4.80	0.307	0.3209	0.159	0.0587
39	11:52:53.04	44:07:11.33	25.0	5.20	0.0	3.1	16.6	4.12	0.0	3.20	0.540	0.5676	-0.664	0.6979
41	11:52:51.95	44:05:47.44	63.0	8.12	5.9	2.45	36.3	6.08	21.0	4.69	0.483	0.2248	-0.243	0.0747
42	11:52:51.60	44:03:43.92	16.3	4.24	0.0	3.1	6.9	2.65	3.6	2.00	0.233	0.2570	-0.202	0.1465
43	11:52:51.14	44:04:41.94	21.2	4.80	0.0	3.1	9.8	3.16	7.6	2.83	0.316	0.3397	-0.104	0.0563
45	11:52:50.80	44:06:53.31	8.1	3.16	0.0	3.1	0.0	4.90	6.1	2.65	0.222	0.3260	0.753	0.8721
46	11:52:50.58	44:06:27.82	16.7	4.24	0.0	3.1	7.8	2.83	8.7	3.00	0.281	0.3078	0.054	0.0302
47	11:52:50.52	44:04:35.66	94.1	9.95	0.0	3.1	37.7	6.25	53.9	7.48	0.368	0.3747	0.172	0.0414
49	11:52:50.39	44:08:06.18	107.4	10.86	7.2	2.83	52.2	7.28	42.4	6.71	0.419	0.1798	-0.091	0.0213
50	11:52:50.23	44:07:11.25	26.1	5.39	7.6	2.83	14.3	3.87	5.6	2.45	0.257	0.1295	-0.333	0.1848
51	11:52:49.59	44:07:16.27	36.0	6.00	2.7	1.73	13.4	3.74	7.1	2.83	0.297	0.2143	-0.175	0.0907
52	11:52:49.01	44:07:17.40	15.2	4.12	0.0	3.1	9.8	3.16	4.5	2.24	0.441	0.4783	-0.349	0.2274
53	11:52:48.92	44:05:28.44	20.3	4.69	0.0	3.1	0.0	4.90	17.5	4.24	0.089	0.1271	0.862	0.9091
56	11:52:47.19	44:06:58.65	16.2	4.24	5.8	2.45	8.7	3.00	2.6	1.73	0.179	0.1083	-0.377	0.2989
58	11:52:46.86	44:10:07.77	16.2	5.00	0.0	3.1	6.6	2.65	0.0	3.20	0.216	0.2422	-0.407	0.4567
59	11:52:46.74	44:09:03.59	13.4	4.12	0.0	3.1	5.7	2.45	0.0	3.20	0.194	0.2195	-0.425	0.4811
60	11:52:46.65	44:06:48.45	354.5	19.13	43.0	6.63	181.2	13.60	132.1	11.70	0.390	0.0701	-0.139	0.0177
61	11:52:46.44	44:07:53.24	46.8	7.28	3.7	2.00	27.2	5.29	13.8	3.87	0.502	0.2988	-0.286	0.1074
62	11:52:46.33	44:03:52.53	10.0	3.32	4.9	2.24	4.9	2.24	0.0	3.20	0.000	0.0000	-0.170	0.1953
63	11:52:46.26	44:06:27.71	92.7	9.80	9.7	3.16	49.2	7.07	34.0	5.92	0.426	0.1583	-0.164	0.0409
64	11:52:45.64	44:05:26.68	13.8	3.87	2.9	1.73	7.9	2.83	2.7	1.73	0.362	0.2718	-0.377	0.2961
65	11:52:44.47	44:09:14.20	19.5	5.00	0.0	3.1	7.8	2.83	9.5	3.32	0.241	0.2637	0.087	0.0493
70	11:52:38.95	44:06:02.49	21.5	4.80	0.0	3.1	8.9	3.00	10.5	3.32	0.270	0.2910	0.074	0.0382
77	11:52:34.44	44:05:16.27	10.7	3.46	0.0	3.1	4.9	2.24	5.6	2.45	0.168	0.1928	0.065	0.0465
Epoch 1: Outside D25 circle														
4	11:53:26.52	44:10:34.65	10.1	4.00	0.0	3.1	0.0	4.90	0.0	3.20	0.178	0.2617	-0.168	0.2472
5	11:53:22.09	44:07:29.95	55.8	8.66	0.0	3.1	22.2	4.90	27.4	5.92	0.342	0.3545	0.093	0.0322
6	11:53:21.57	44:11:31.38	43.9	8.60	0.0	3.1	19.1	4.80	25.8	6.08	0.364	0.3825	0.153	0.0605
9	11:53:11.74	44:07:03.09	25.9	6.25	0.0	3.1	6.4	2.83	12.0	4.00	0.127	0.1427	0.216	0.1306
10	11:53:11.11	43:57:19.53	73.6	9.85	0.0	3.1	32.0	6.16	32.1	6.32	0.393	0.4033	0.001	0.0004
11	11:53:09.67	44:00:04.79	29.2	6.86	0.0	3.1	14.0	4.00	16.5	4.90	0.373	0.3980	0.086	0.0406
12	11:53:09.05	44:03:00.92	16.1	5.39	0.0	3.1	10.2	3.32	0.0	3.20	0.441	0.4867	-0.634	0.6992
14	11:53:07.46	44:02:19.47	84.3	9.95	13.0	3.74	41.3	6.63	30.5	5.83	0.336	0.1175	-0.128	0.0354
16	11:53:07.05	43:58:58.78	27.3	6.00	0.0	3.1	14.8	4.00	8.7	3.32	0.429	0.4538	-0.223	0.1155
17	11:53:06.57	44:02:36.21	39.8	7.68	0.0	3.1	0.0	4.90	28.6	5.74	0.045	0.0646	0.719	0.7459
19	11:53:05.81	44:03:34.88	81.3	9.27	2.6	1.73	32.5	5.74	47.6	7.00	0.368	0.2566	0.186	0.0477
25	11:52:59.72	44:02:12.99	12.0	4.00	0.0	3.1	0.0	4.90	0.0	3.20	0.150	0.2179	-0.142	0.2058
66	11:52:44.20	43:59:14.67	25.0	6.56	0.0	3.1	0.0	4.90	12.3	4.00	0.072	0.1036	0.492	0.5332

Table 11 continued on next page

Table 11 (continued)

N	RA	Dec	BCts	BUnc	SCTs	SUnc	MCts	MUnc	HCts	HUnc	M-S/B	UM-S/B	H-M/B	UH-S/B
69	11:52:39.35	44:03:27.68	37.4	6.71	5.9	2.45	11.7	3.46	6.1	2.65	0.155	0.0838	-0.150	0.0831
71	11:52:38.93	43:58:52.25	24.1	6.33	0.0	3.1	0.0	4.90	25.0	5.66	0.075	0.1074	1.037	1.0979
72	11:52:38.72	44:12:46.71	297.7	18.47	31.1	6.08	136.0	12.04	129.9	12.25	0.352	0.0787	-0.020	0.0029
75	11:52:36.43	44:01:07.42	17.6	5.39	0.0	3.1	6.2	2.65	8.0	3.32	0.176	0.1990	0.102	0.0685
78	11:52:28.24	44:11:06.32	17.4	5.57	0.0	3.1	0.0	4.90	0.0	3.20	0.103	0.1500	-0.098	0.1417
79	11:52:27.12	44:04:54.49	18.1	4.69	0.0	3.1	8.9	3.00	7.7	3.00	0.320	0.3482	-0.066	0.0382
80	11:52:25.04	44:07:22.40	22.2	6.25	0.0	3.1	12.4	3.61	0.0	3.20	0.419	0.4520	-0.559	0.6026
82	11:52:21.44	44:12:08.93	35.2	7.28	0.0	3.1	13.2	4.00	19.6	5.39	0.287	0.3056	0.182	0.0834
83	11:52:18.05	44:00:42.87	26.1	6.71	0.0	3.1	0.0	4.90	14.7	4.58	0.069	0.0991	0.563	0.6074
84	11:52:15.28	44:09:20.71	26.7	6.86	11.7	3.61	12.5	3.74	0.0	3.20	0.030	0.0150	-0.348	0.3744
85	11:52:14.41	44:00:40.70	47.2	8.37	0.0	3.1	13.0	3.87	31.9	6.56	0.210	0.2220	0.400	0.1613
86	11:52:13.11	44:01:28.22	63.7	9.33	0.0	3.1	32.1	6.00	26.1	5.83	0.455	0.4679	-0.094	0.0307
87	11:52:13.11	44:09:02.54	110.4	12.73	0.0	3.1	47.1	7.35	56.0	8.37	0.399	0.4060	0.081	0.0197
89	11:52:09.24	44:04:22.25	28.5	6.78	0.0	3.1	17.8	4.47	0.0	3.20	0.516	0.5458	-0.625	0.6609
90	11:52:04.12	44:08:10.54	26.1	7.14	0.0	3.1	9.8	3.46	0.0	3.20	0.257	0.2811	-0.375	0.4112
91	11:52:04.06	44:11:29.88	44.4	9.38	9.2	3.46	30.2	6.71	0.0	3.20	0.473	0.2295	-0.608	0.6360
92	11:52:01.68	44:03:13.27	84.5	12.45	0.0	3.1	41.7	6.93	29.9	7.21	0.457	0.4679	-0.140	0.0458
93	11:51:57.46	44:05:21.48	39.1	8.72	0.0	3.1	0.0	4.90	39.1	8.72	0.046	0.0659	1.000	1.0486
94	11:51:54.01	44:07:55.66	22.3	6.93	0.0	3.1	7.1	3.00	0.0	3.20	0.179	0.2025	-0.318	0.3595
95	11:51:50.98	43:59:59.96	33.5	7.88	0.0	3.1	28.9	6.71	0.0	3.20	0.770	0.8111	-0.863	0.9086

^a Column headings for this and the next table are defined as follows: 'N' = source number from the *merged* source list; 'RA', 'Dec' = source position, J2000, in descending RA order; 'BCts' = Broad band Counts; 'BUnc' = Broad band counts UNCertainty; similarly for S, M, and H = Soft, Medium, Hard bands; 'M-S/B' = (M - S)/B; UM-S/B = Uncertain of (M - S)/B; and similarly for 'H-M/B' and 'UH-M/B'. The equation columns were compressed (smaller font, fewer characters) to allow the tables to fit on the page.

Table 12. Color-Color Results By Source: Epoch 2^a

N	RA	Dec	BCts	BUnc	SCts	SUnc	MCts	MUnc	HCts	HUnc	M-S/B	UM-S/B	H-M/B	UH-S/B
Within D25 circle														
21	11:53:03.92	44:08:46.46	15.6	4.12	0.0	3.60	10.7	3.32	0.0	4.50	0.4551	0.4915	-0.3974	0.4292
23	11:53:00.25	44:06:00.43	54.5	7.48	0.0	3.60	27.7	5.29	21.1	4.69	0.4422	0.4543	-0.1211	0.0392
26	11:52:57.58	44:06:47.34	10.6	3.46	0.0	3.60	6.8	2.65	4.7	2.24	0.3019	0.3387	-0.1981	0.1380
29	11:52:55.24	44:09:05.08	14.1	4.24	0.0	3.60	0.0	2.60	8.6	3.16	-0.0709	0.1025	0.4255	0.4711
30	11:52:54.84	44:07:36.10	8.6	3.16	0.0	3.60	0.0	2.60	6.3	2.65	-0.1163	0.1699	0.4302	0.4928
31	11:52:54.76	44:09:17.18	10.0	3.61	4.5	2.24	0.0	2.60	0.0	4.50	-0.1900	0.2230	0.1900	0.2773
32	11:52:54.70	44:07:52.34	72.9	8.78	2.9	1.73	36.0	6.08	32.2	5.83	0.4540	0.2868	-0.0521	0.0144
33	11:52:54.68	44:05:29.09	15.0	4.00	0.0	3.60	8.9	3.00	5.6	2.45	0.3533	0.3846	-0.2200	0.1349
34	11:52:54.46	44:06:58.67	14.8	4.00	0.0	3.60	6.9	2.65	7.6	2.83	0.2230	0.2463	0.0473	0.0283
37	11:52:53.71	44:07:34.74	18.9	4.58	0.0	3.60	3.8	2.00	13.9	3.87	0.0106	0.0122	0.5344	0.3435
38	11:52:53.49	44:06:12.83	27.9	5.48	0.0	3.60	11.7	3.46	14.1	3.87	0.2903	0.3081	0.0860	0.0386
41	11:52:51.92	44:05:47.92	23.8	5.00	0.0	3.60	10.7	3.32	13.7	3.74	0.2983	0.3186	0.1261	0.0584
43	11:52:51.13	44:04:42.57	30.3	6.08	0.0	3.60	13.0	3.74	10.4	3.46	0.3102	0.3288	-0.0858	0.0415
46	11:52:50.57	44:06:28.33	9.8	3.32	0.0	3.60	2.6	1.73	5.6	2.45	-0.1020	0.1273	0.3061	0.2649
47	11:52:50.52	44:04:36.26	87.3	9.59	0.0	3.60	32.0	5.74	56.0	7.68	0.3253	0.3324	0.2749	0.0690
49	11:52:50.34	44:08:06.64	66.8	8.37	0.0	3.60	30.4	5.57	33.4	5.92	0.4012	0.4110	0.0449	0.0128
50	11:52:50.22	44:07:11.63	25.1	5.29	0.0	3.60	18.4	4.36	5.0	2.45	0.5896	0.6186	-0.5339	0.3116
51	11:52:49.56	44:07:17.22	17.6	4.58	0.0	3.60	7.4	2.83	0.0	4.50	0.2159	0.2379	-0.1648	0.1815
52	11:52:48.98	44:07:17.75	13.7	4.00	5.5	2.45	7.4	2.83	7.2	2.83	0.1387	0.0909	-0.0146	0.0091
53	11:52:48.91	44:05:28.67	14.8	4.00	0.0	3.60	0.0	2.60	12.6	3.61	-0.0676	0.0973	0.6757	0.7262
54	11:52:48.10	44:07:03.70	9.3	3.32	0.0	3.60	0.0	2.60	6.2	2.65	-0.1075	0.1568	0.3871	0.4431
56	11:52:47.20	44:06:59.15	7.5	3.00	0.0	3.60	6.6	2.65	0.0	4.50	0.4000	0.4598	-0.2800	0.3218
59	11:52:46.65	44:09:04.67	12.2	4.00	3.7	2.00	0.0	2.60	0.0	4.50	-0.0902	0.1067	0.1557	0.2261
61	11:52:46.48	44:07:53.85	60.5	8.12	3.6	2.00	31.0	5.66	24.3	5.10	0.4529	0.2717	-0.1107	0.0342
63	11:52:46.24	44:06:28.30	54.3	7.68	0.0	3.60	30.3	5.57	18.1	4.47	0.4917	0.5048	-0.2247	0.0761
65	11:52:44.46	44:09:14.94	26.3	5.57	0.0	3.60	11.6	3.46	15.6	4.24	0.3042	0.3239	0.1521	0.0693
74	11:52:36.88	44:07:56.70	19.9	6.33	0.0	3.60	0.0	2.60	0.0	4.50	-0.0503	0.0728	0.0955	0.1384
Epoch 2: Outside D25 circle														
1	11:53:54.95	44:00:39.43	17.8	5.57	0.0	3.60	11.7	3.87	0.0	4.50	0.4551	0.5000	-0.4045	0.4445
2	11:53:42.85	44:07:15.65	42.7	7.94	0.0	3.60	21.1	5.00	18.5	5.20	0.4098	0.4280	-0.0609	0.0251
3	11:53:27.49	44:10:33.19	24.8	6.33	0.0	3.60	7.5	3.00	16.1	5.10	0.1573	0.1741	0.3468	0.1978
4	11:53:26.35	44:10:36.64	14.8	5.20	0.0	3.60	8.6	3.16	0.0	4.50	0.3378	0.3790	-0.2770	0.3108
5	11:53:21.96	44:07:30.69	20.9	5.00	0.0	3.60	8.5	3.00	8.8	3.16	0.2344	0.2549	0.0144	0.0080
6	11:53:21.61	44:11:31.16	32.2	6.40	0.0	3.60	20.2	4.58	0.0	4.50	0.5155	0.5385	-0.4876	0.5093
7	11:53:18.99	44:12:14.52	17.3	5.39	0.0	3.60	11.7	3.61	0.0	4.50	0.4682	0.5112	-0.4162	0.4544
8	11:53:18.92	44:00:30.15	21.2	6.08	0.0	3.60	0.0	2.60	0.0	4.50	-0.0472	0.0681	0.0896	0.1293
9	11:53:11.85	44:07:02.53	11.6	3.61	0.0	3.60	6.9	2.65	0.0	4.50	0.2845	0.3173	-0.2069	0.2308
12	11:53:09.22	44:03:01.57	19.6	5.00	0.0	3.60	10.2	3.32	9.3	3.46	0.3367	0.3644	-0.0459	0.0255
14	11:53:07.38	44:02:20.37	38.7	6.93	0.0	3.60	17.2	4.36	15.6	4.36	0.3514	0.3680	-0.0413	0.0173
15	11:53:07.39	44:04:50.65	14.1	4.00	0.0	3.60	5.8	2.45	7.2	2.83	0.1560	0.1751	0.0993	0.0638
16	11:53:07.03	43:59:00.44	25.6	6.86	0.0	3.60	18.0	4.58	0.0	4.50	0.5625	0.5997	-0.5273	0.5622
19	11:53:05.80	44:03:34.66	34.8	6.16	0.0	3.60	14.1	3.87	20.5	4.69	0.3017	0.3174	0.1839	0.0733
20	11:53:04.03	44:10:22.25	25.5	5.48	0.0	3.60	11.4	3.46	9.5	3.46	0.3059	0.3263	-0.0745	0.0388
25	11:52:59.85	44:02:13.49	28.5	6.48	0.0	3.60	14.6	4.00	12.6	4.36	0.3860	0.4097	-0.0702	0.0348
68	11:52:40.71	44:11:09.34	15.5	1.00	0.0	3.60	6.5	2.65	10.3	3.87	0.1933	0.2189	0.2533	0.1648
72	11:52:38.75	44:12:47.34	326.9	19.29	27.1	5.39	149.2	12.53	151.5	13.12	0.3735	0.0836	0.0070	0.0009
76	11:52:35.96	43:57:25.09	32.4	7.55	0.0	3.60	16.6	4.80	13.0	4.58	0.4012	0.4280	-0.1111	0.0569

Table 12 continued on next page

Table 12 (*continued*)

N	RA	Dec	BCts	BUnc	SCts	SUnc	MCts	MUnc	HCts	HUnc	M-S/B	UM-S/B	H-M/B	UH-S/B
84	11:52:15.20	44:09:20.64	18.8	5.83	12.2	3.74	0.0	2.60	0.0	4.50	-0.5106	0.5571	0.1011	0.1463
87	11:52:12.97	44:09:01.63	50.6	8.95	0.0	3.60	11.6	3.87	38.7	7.68	0.1581	0.1690	0.5356	0.2285

^aSee Table 11 for the column definitions which are identical to the columns in this table.

REFERENCES

- Bekhti et al. 2016, *A&A*, 594, A116
- Bertin, E. & Arnouts, S. 1996 *A&AS*, 117, 393
- Bianchi, L. 2014, *Ap&SS*, 354, 103
- Binder, B.; Gross, J.; Williams, B. F. et al. 2017, *ApJ*, 834, 128
- Brandt, W. N. et al. 2001, *AJ*, 122, 2810
- Buhidar, K. & Schlegel, E. M. 2017, *BAAS*, 22914412
- Caldú-Primo, A., Cruz-González, I.; & Morisset, C. 2009, *A&A*, 493, 33
- Calzetti, D., Kennicutt, R. C., Engelbracht, C. W., et al. 2007, *ApJ*, 666, 870
- Campana, S., Moretti, A., Lazatti, D., & Tagliaferri, G. 2001, *ApJ*, 560, L19
- Chandar, R.; Johns, P.; Mok, A.; Prestwich, A.; Gallo, E.; & Hunt, Q. 2020, *ApJ*, 890, 150
- Charles, P.A. & Seward, F.D. 1995, *Exploring the X-ray Universe* (Cambridge: Cambridge Univ Press)
- Dale, D. A., Gil de Paz, A.; et al. 2007, *ApJ*, 655, 863
- Evans, I. N., Primini, F. A., Glotfelty, K. J. et al. 2010, *ApJS*, 189, 37
- Fabbiano, G. & Elvis, M. 2019, *ApJ*, 884, 163.
- Fabbiano, G.; Kim, D.-W.; & Trinchieri, G. 1992, *ApJS*, 80, 531
- Fazio, G. G., Hora, J. L., Allen, L. E. et al. 2003 *ApJS*, 154, 10
- Freeman, P. E., Kashyap, V.; Rosner, R.; & Lamb, D. Q. 2002 *ApJS*, 138, 185
- Fruscione, A., et al. 2006, *Proc. SPIE*, 6270
- , Gaetz, T. J.; Jerius, D.; Edgar, R. J.; Van Speybroeck, L. P.; Schwartz, D. A.; Markevitch, M. L.; Taylor, S. C.; & Schulz, N. S. 2000, *SPIE*, 4012, 41
- Garmire, G.; Bautz, M. W.; Ford, P. G.; Nousek, J. A.; & Ricker, Jr., G. R. 2003 *SPIE*, 4851, 28
- Gilfanov, M. 2004, *MNRAS*, 349, 146
- Gregory, P. C. & Loredó, T. J. 1992, *ApJ*, 398, 146
- Grimm, H.-J., Gilfanov, M. & Sunyaev, R. 2003, *MNRAS*, 339, 793
- Hamilton, A.J.S. & Sarazin, C. L. 1984, *ApJ*, 284, 601
- Ho, L., Filippenko, A. V., & Sargent, W. L. W. (1997), *ApJS*, 112, 315
- Hunt, Q.; Gallo, E.; Chandar, R.; Mulia, P. J.; Mok, A.; Prestwich, A.; & Liu, S. 2021, *ApJ*, 912, 31
- Hunt, Q.; Gallo, E.; Chandar, R.; Mok, A.; & Prestwich, A. 2023, *ApJ*, 947, 31
- Hunt, Q.; Chandar, R.; Gallo, E.; Floyd, M.; Maccarone, T. J.; & Thilker, D. A. 2023, *ApJ*, 953, 126
- Jimenez-Vicente, J.; Battaner, E.; Rozas, M.; Castenada, H.; & Poncel, C. 1999, *A&A*, 342, 417
- Kennicutt, R. C. Jr.; Hao, C.-N.; Calzetti, D.; Moustakas, J.; Dale, D. A.; Bendo, G.; Engelbracht, C. W.; Johnson, B. D.; & Lee, J. C. 2009, *ApJ*, 703, 1672
- Kennicutt, R. C. & Kent, S. M. 1983, *AJ*, 88, 1094
- Kim, D.-W.; et al. 2007, *ApJS*, 169, 401
- Lee, H., Skillman, E. D., Cannon, J. M., et al. 2006, *ApJ*, 647, 970
- Lehmer, B.; Eufrazio, R. T.; Basu-Zych, A. et al. 2021, *ApJ*, 907, 17
- Lehmer, B.; Eufrazio, R. T.; Tzanavaris, P. et al. 2019, *ApJS*, 243, 3
- Long, K. 2020, in *Handbook of Supernovae*, Alsabti, A. W. & Murdin, P. (eds) (SpringerLink) (also arXiv 1712.05331)
- Marchesi, S., Gilli, R., Lanzuisi, G. et al. 2020, *A&A*, 642, A184
- Marin, F. et al. 2023, *Nature*, 619, 41
- MAST Portal Guide, eds. R. A. Shaw, B. Cherinka, P. Forshay (ver 2; Baltimore: STScI)
- Mineo, S., Gilfanov, M. & Sunyaev, R. 2012, *MNRAS*, 419, 2095
- Mushotzky, R. F., Cowie, L. L., Barger, A. J., & Arnaud, K. A. 2000, *Nature*, 404, 459
- Pannuti, T. G., Swartz, D. A., Laine, S., Schlegel, E. M., Lacey, C. K., Moffitt, W. P., Sharma, B., Lackey-Stewart, A. M., Kosakowski, A. R., Filipović, M. D., & Payne, J. L. 2015, *AJ*, 150, a91
- Pellegrini, S., Cappi, M. et al. 2000, *A&A*, 353, 447
- Portegies Zwart, S. F., McMillan, S. L. W., & Makino, J. 2007, *MNRAS*, 374, 95
- Poznanski, D.; Butler, N. et al. 2009, *ApJ*, 694, 1067
- Prestwich, A. 2004, *RMxAC*, 20, 3
- Prestwich, A. et al. 2003, *ApJ*, 595, 719
- Rieke, G. H.; Young, E. T.; Engelbracht, C. W. et al. 2004, *ApJS*, 154, 25
- Rodriguez, O., Clochiatti, A., & Hamuy, M. 2014, *AJ*, 148, 107
- Rosati, P. et al. 2002, *ApJ*, 566, 667
- Sasaki, M. 2020, *AN*, 341, 156
- Satyapal, S.; Vega, D.; Dudik, R. P.; Abel, N. P. & Heckman, T. 2008, *ApJ*, 677, 926
- Schlegel, E. M. & Pannuti, T. G. 2003, *AJ*, 125, 3025
- Soria, R. & Wu, K. 2003, *A&A*, 410, 53
- Swartz, D.; Ghosh, K. K.; McCullough, M. L. et al. 2003, *ApJS*, 144, 213
- Thornley, M. D. 2004 in *Dense Interstellar Medium in Galaxies*, ed. S. Pfalzner et al. (Berlin: Springer), p109
- Townsley, L. K., Feigelson, E. D., Montmerle, T. et al. 2003, *ApJ*, 593, 874

- Tully, R. B. & Shaya, E. J.. 1984, ApJ, 281, 31
- Van Dyk, S.; Filippenko, A., Fox, O. D. et al. 2017, ATEL 10485
- van Speybroeck, L. P.; Jerius, D.; Edgar, R. J.; Gaetz, T. J.; Zhao, P.; & Reid, P. B. 1997 SPIE, 3113, 89
- Weisskopf, M. C., Brinkman, B., Canizares, C.; Garmire, G.; Murray, S.; & Van Speybroeck, L. P. 2002 PASP, 114, 1
- Werner, M. W.; Roellig, T. L. Low, F. S. et al. 2004 ApJS, 154, 1
- Zampieri, L. 2006, MSAIS, 9, 378
- Zaritsky, D.; Kennicutt, R. C. Jr.; Huchra, J. P. 1994, ApJ 420, 87

